JOURNAL OF GEOPHYSICAL RESEARCH, VOL. 100, NO. B4, PAGES 6005–6024, APRIL 10, 1995

# Dike intrusion as a trigger for large earthquakes and the failure of volcano flanks

Derek Elsworth

Department of Mineral Engineering, Pennsylvania State University, University Park

Barry Voight

Department of Geosciences, Pennsylvania State University, University Park

**Abstract.** Pore fluid pressures induced through dike intrusion have the capability to trigger large earthquakes and to initiate and sustain massive and catastrophic failure of volcano flanks. Suprahydrostatic pore pressures are generated as a result of both mechanical and thermal straining of the rock-fluid medium. Mechanical strains and resulting pore pressures are described using an analogy to a moving volumetric dilation within a porous elastic medium. Thermal pore fluid pressures are simply represented by a static diffusive model subjected to uniform temperature rise at the dike interface. Resulting excess pore pressure distributions acting along the base of a wedge-shaped slide block are used to define the stability of the flanks when subjected to the magma pressures that accompany intrusion. The destabilizing influence of mechanically induced pore pressures is maximized as the intruded width, or corresponding overpressure, of the dike is increased. For realistic parameter magnitudes in volcaniclastic materials, induced pore pressures are capable of initiating failure; however, the mechanical influence is restricted to the proximity of the intrusion, and by itself may not be capable of sustaining sliding motion once it is initiated. The destabilizing influence of thermally induced pore pressures is conditioned by the severity of thermal forcing, ratios of thermal and hydraulic diffusivities, and the time available for the combined thermal and pressure disturbance to propagate outward from the dike. Thermal pressurization of pore fluid extends more slowly than mechanical straining but is shown to be capable of developing massive uplift forces that could initiate and possibly sustain failure along downslope-dipping failure planes. Deviatoric stress-induced generation of pore pressures and frictional heating of pore fluids may act following slide initiation to maintain the impetus of flank failure and enable long runout over compressible marine sediments. In addition to the development of shallow failure, limited deep-seated sliding may also result from the mechanical or thermal pore pressure loading mechanisms. In addition, pore pressures generated through intrusion or frictional heating may trigger, or amplify, large earthquakes, and these in turn may aid shallower flank slip through seismic ground accelerations and vibration-induced pore pressure generation. These phenomenological models of pore pressure rise and stability control may aid comprehension of the cyclic growth, lateral expansion, and subsequent destruction of shield and stratovolcano flanks. Examples in this work refer particularly to oceanic volcanoes typified by the Hawaiian Islands and Réunion Island.

## Introduction

The agents of volcanism not only produce the growth of volcanic edifices but also contribute to their cyclic destruction by giganitic landslides. Such landslides occur on many volcanoes widely spread over the Earth, representing a process of wide significance [*Holcomb and Searle,* 1993]. Some are greater than 5000 km$^3$, large enough to displace half of the subaerial fraction and 20% of the total volcanic edifice [*Moore et al.,* 1989].

Dike injection provides a mechanism to assist the initiation of debris avalanches and deep flank slip, by creating a magma wedge that severs the updip attachment of the slide block and exerts substantial magma pressure on the head wall [*Voight,* 1972; *Gucwa and Kehle,*



Paper number 94JB02884.
0148-0227/95/94JB-02884$05.00

1978; *Prostka,* 1978]. The basic idea may be traced to *Hall* [1815]; a magmatically augmented driving force provides a viable means to explain lateral slip in Hawaii [*Lipman et al.* 1985; *Dieterich,* 1988], although both the mechanisms of failure and of long runout appear "mechanically enigmatic" because of frictional resistance [*Iverson,* 1991]. *Iverson* [1992, 1995] considered several conditions "under which large scale failures might occur," including gravity driven hydraulic gradients, relative sea-level changes and gravitational consolidation due to a growing volcano mass, possibly in combination with excess magma pressure. He concluded, however, that these mechanisms were insufficient to cause large scale failure, and therefore "a simple, quantitative explanation for failure of Hawaiian volcano flanks remains elusive."

We hypothesize that the pressurization of pore fluids accompanying dike intrusion can be a sufficient additional trigger mechanism for both the deep and shallow flank slip events, and for associated earthquakes. Magma overpressure augments the forces driving failure, and indirectly reduces the resistance along the basal failure plane through several mechanisms of pore fluid pressurization [*Voight and Elsworth,* 1992].

Pore fluid pressurization in association with volcanic activity has been observed at several localities [*Björnsson et al.,* 1977; *Stefánsson,* 1981; *Watanabe,* 1983]. Such episodes of fluid pressurization may result jointly from the mechanical and thermal strain fields that are induced in saturated porous country rock by dike intrusion. These dual mechanisms for pore pressure generation act additively on potential basal failure planes, with the net effect of decreasing Terzaghian effective stresses and consequently decreasing the frictional resistance to failure. In addition, pore pressures generated through dike intrusion, at depth, may trigger large earthquakes and these in turn may aid the processes of flank slip through shaking-induced pore pressure generation and ground acceleration.

These agents of pore pressure generation provide a rational, and quantifiable, means of sustaining the reduction in basal shear strength, even as the driving forces provided by magma pressurization ultimately drop as flank displacement occurs. Other mechanisms, including induced generation of pore pressures through pore collapse [*Skempton,* 1954], undrained loading [*Hutchinson and Bhandari,* 1971], and frictional-heat fluid pressurization [*Voight and Faust,* 1982] beneath the displaced slope may all act following slide initiation to maintain, and perhaps accelerate, the impetus of flank failure.

The concurrent pressurization mechanisms of mechanical and thermal straining of the solid and fluid constituents of the surrounding medium are intrinsically coupled but, for convenience and tractability, may be considered independently as a reasonable first order-estimate.

## Mechanically Generated Pore Pressures

### Introduction

When magma is intruded within a saturated porous medium, it strains the surrounding medium. This strain, in turn, produces changes in pore fluid pressures that may dissipate with time. Dike intrusion is a dynamic process that may be approximated by the behavior of a moving volumetric dislocation [*Cleary,* 1977, 1978; *Rudnicki,* 1981]. This approach has been applied to represent the pore pressure fields induced during intrusive events at Krafla, Iceland [*Elsworth and Voight,* 1992].

Depending on the specific geometry of the dike, the volumetric dislocation may be a point or line dislocation, representing the essential geometries of a pencil (conduit) or of a blade (infinite planar dike), respectively. These are end-members of all intermediate geometries. In addition, adequately representing the velocity of propagation of the dike is important in defining the morphology of the induced pressure bulb around the dike front; the physical situation differs considerably from the case where instantaneous intrusion is assumed [*Elsworth and Voight,* 1992].

For both the pencil and blade dike geometries, the induced pore fluid pressures reach a steady state when viewed relative to the migrating dislocation or dike front. Although the fully transient pore pressure field may be evaluated, this steady representation is adequate for characterizing pore pressure changes at Krafla [*Elsworth and Voight,* 1992]. We assume steady behavior. For brevity, the form of a planar dike is selected as most representative of the geometry in an intruded volcano flank.

### Planar Dike

For a planar dike, of infinite extent in the $y$ direction (Figure 1), the steady distribution of dimensionless pressure, $P_D^m$, around the advancing dislocation front is given as [*Elsworth and Voight,* 1992]

$$P_D^m = K_0[U_D R_D] e^{U_D x_D} \tag{1}$$

where $K_0[x]$ is the modified Bessel function of the second kind of zero order. Dimensionless pressure, $P_D^m$, is controlled by the dimensionless intrusion velocity, $U_D$, and geometric variables $R_D$ and $x_D$, illustrated in the geometry of Figure 1. For the planar dike, these variables are defined as

$$P_D^m = \frac{2\pi(p - p_s)}{Uw} \frac{k}{\mu} \tag{2}$$

$$U_D = \frac{U h_s}{2c} \tag{3}$$

$$(x_D,\ y_D,\ z_D) = \frac{1}{h_s}(x,\ y,\ z) \tag{4}$$

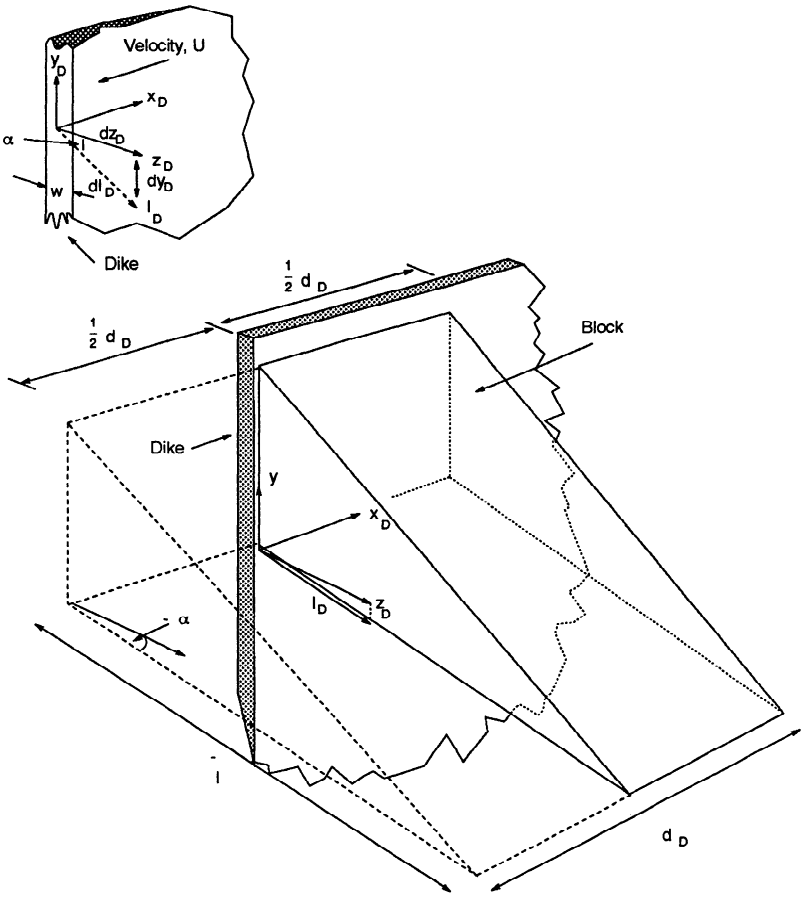


**Figure 1.** Geometry of a planar dike and of its front at $x_D = 0$ and with a coordinate system that migrates with the moving dike front. The dike width is $w$, and the front moves with velocity $U$. Mechanically induced pressures are desired on a plane striking parallel to the dike migration direction and inclined at $\alpha$ degrees to the horizontal ($z$ axis). The limits of integration are the extent of the basal failure plane, given as 0 to $\bar{l}_D$ and $-\frac{1}{2}d_D$ to $+\frac{1}{2}d_D$, where $\bar{l}_D$ is the length of the basal failure plane.

and

$$R_D^2 = x_D^2 + z_D^2. \tag{5}$$

The parameters comprising these dimensionless groups are width of the intruded dike, $w$, initial pore fluid pressure, $p_s$, total pore fluid pressure following intrusion, $p$, propagation velocity of the dike front, $U$, permeability of the porous medium, $k$, dynamic viscosity of the saturating fluid, $\mu$, and hydraulic diffusivity of the porous medium, $c$. Height of the slope crest above sea level, $h_s$, is as defined later in Figure 3. The pore pressure distribution remains constant with time, relative to the coordinate system that migrates with the dislocation front.

Under the hypothesis that intrusion-induced pore pressures may trigger flank instability, the distribution of induced fluid pressures on a plane inclined relative to the dike is of primary importance. For failure along an inclined plane striking parallel with the dike (Figure 4), the pressure distribution of interest is that on trace $l$ inclined at angle $\alpha$ with respect to the horizontal ($z_D$ direction), as illustrated in Figure 1. The normalized trace length is $l_D^2 = y_D^2 + z_D^2$ with $l_D = l/h_s$. The angle is defined as positive counterclockwise from the positive $z_D$ axis. The uplift force, $F_{p_m}$, acting along this trace may be determined by integrating the pressure distribution of equation (1) as

$$\begin{aligned} F_{p_m} &= \int_{-\frac{1}{2}d}^{+\frac{1}{2}d} \int_0^{\bar{l}} (p - p_s) dl dx \\ &= w_D U_D \gamma_w h_s^3 \int_{-\frac{1}{2}d_D}^{+\frac{1}{2}d_D} \int_0^{\bar{l}_D} P_D^m dl_D dx_D \end{aligned} \tag{6}$$

illustrating that the magnitude of the uplift force is modulated by a dimensionless dike width, $w_D$, as

$$w_D = \frac{\mu}{k} \frac{wc}{\pi \gamma_w h_s^2} \tag{7}$$

where $\bar{l}_D$ is the limit of integration measured along the trace and $\gamma_w$ is the unit weight of water. The normalized length of integration along the $x$ axis, representing the path of dike propagation, is $d_D = d/h_s$ with $d$ representing the actual width of the failure block. Dike width, $w_D$, may be thought of as a dimensionless dike

thickness since, for a given intrusion location, all other parameters are fixed material properties. The limits of integration of equation (6) may be changed on noting from Figure 1 that $dl_D = dz_D/\cos\alpha$. Substituting this and equation (2) into equation (6) yields

$$\bar{F}_{p_m} = \frac{w_D U_D}{\cos\alpha}\int_{-\frac{1}{2}d_D}^{+\frac{1}{2}d_D}\int_0^{\bar{l}_D\cos\alpha} K_0[U_D R_D] \cdot e^{U_D x_D} dz_D dx_D \quad (8)$$

where $\bar{F}_{p_m} = F_{p_m}/\gamma_w h_s^3$. Further, by using the substitution $\eta = U_D R_D$,

$$dz_D = \frac{R_D}{U_D z_D} d\eta \quad (9)$$

and

$$\bar{F}_{p_m} = \frac{w_D}{\cos\alpha}\int_{-\frac{1}{2}d_D}^{+\frac{1}{2}d_D}\int_{\frac{1}{2}U_D d_D}^{U_D\bar{R}_D} K_0[\eta] e^{\eta\frac{x_D}{R_D}}\frac{R_D}{z_D} d\eta dx_D \quad (10)$$

and

$$U_D\bar{R}_D = U_D\sqrt{\frac{d_D^2}{4} + \bar{l}_D^2\cos^2\alpha} \quad (11)$$

to give the normalized uplift force applied orthogonal to a rectangular plane inclined at $\alpha$ to the horizontal and of dimension $\bar{l}_D \times d_D$. In the limit, as $\bar{l}_D \to \infty$ and $d_D \to 0$,

$$\int_0^\infty K_0[\eta] d\eta = \frac{\pi}{2} \quad (12)$$

and

$$\frac{\bar{F}_{p_m}\cos\alpha}{w_D} = \frac{\pi}{2} d_D \quad (13)$$

enabling the uplift force to be determined analytically. The form of the pressure distribution is sharply peaked around the origin, and equation (13) is adequate provided $\bar{l}_D$ is sufficiently large to include most of the distributed pressure. From the full form of equation (10), it is also possible to evaluate the length, $\bar{l}_D^{95}$, required such that 95% of the maximum uplift force is included. From numerical evaluation of the integral, this may be approximated as

$$\bar{l}_D^{95} \approx \frac{2.186}{U_D\cos\alpha}. \quad (14)$$

This enables the pressure distribution to be approximated by equation (13) when $d_D$ is sufficiently small. In all other circumstances, equation (10) must be evaluated numerically. Dimensionless uplift force, $\bar{F}_{p_m}$, is defined in terms of the dimensionless groups,

$$\frac{\bar{F}_{p_m}\cos\alpha}{w_D} = f[d_D;\ U_D;\ \bar{l}_D] \quad (15)$$

and must be defined for individual geometries of a sliding block. Where the dimensionless trace length is sufficiently large that $\bar{l}_D$ conforms to the requirements of equation (14), then the dimensionless uplift force may be determined as illustrated in Figure 2. Bounding behavior within the diagram is defined by equation (13), with dike intrusion rate, $U_D$, defining the appropriateness of this approximation. Magnitudes of the uplift force become constant above a threshold width mag-

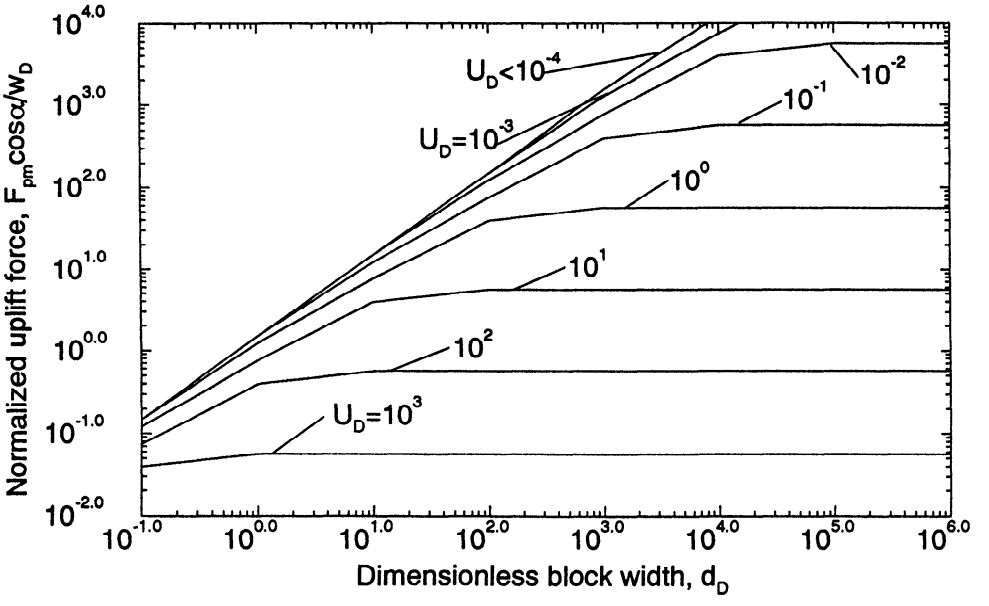


**Figure 2.** Integrated uplift force $\bar{F}_{p_m}$ as a function of dimensionless dike width $d_D$ and dimensionless intrusion rate $U_D$. Note that evaluations assume $\bar{l}_D \to \infty$ and the distribution is not truncated by the finite extent of the basal failure plane.

nitude, $d_D$, defining the effective lateral extent of the induced pressure pulse. For magnitudes of $\bar{l}_D$ significantly less than the limiting value of equation (13), the appropriate trace length of integration must be included in the evaluation. The magnitudes included in Figure 2, however, represent maximum limiting magnitudes of the uplift force.

## Thermally Generated Pore Pressures

Thermal loading of the host rocks, resulting from the emplacement of an intrusion, will also induce increased fluid pressures [*Delaney*, 1982]. A one-dimensional model is consistent with the planar dike geometry used in the preceding and may be used to evaluate the approximate induced pressure distribution on a plane inclined at any angle $\alpha$ to the dike orthogonal. Although more complicated geometries and boundary conditions may be envisaged for specific cases, the model examined here is adequate to explore the basic idea. A simplified expression for dike-induced pressures is available from *Delaney* [1982] for the case where thermal transport is diffusive and results from the application of a temperature change of magnitude, $\Delta T$, applied at $z = z_D = 0$. Under this condition, the change in dimensionless pressure, $P_D^t$, is given as

$$P_D^t = \mathrm{erfc}\left(\frac{Dz_D}{t_D}\right) \tag{16}$$

where $D$ is the ratio of the thermal and hydraulic diffusivities of the medium, $t_D$ is a dimensionless time, and the component parameters are defined as

$$P_D^t = \frac{(p - p_s)}{K_b A D}, \tag{17}$$

$$D = \sqrt{\frac{\kappa n}{c}} \tag{18}$$

and

$$t_D = \frac{4\kappa t}{h_s^2} \tag{19}$$

where $K_b$ is the undrained bulk skeletal modulus of the solid, $A$ is thermal strain, $\alpha_t \Delta T$, where $\alpha_t$ is the coefficient of free thermal expansion, $\kappa$ is thermal diffusivity, $n$ is porosity, $t$ is time, $c$ is hydraulic diffusivity, and $z_D$ is the dimensionless lateral distance from the intrusion, as $z_D = z/h_s$.

In this evaluation, we ignore the convective transport that results from thermal strain, from transfer of gas exsolved from magma into groundwater, or from the fluid pressure gradients mechanically induced by intrusion. These assumptions appear reasonable for a porous medium where pressure gradients remain moderate and, correspondingly, Peclet numbers remain considerably less than unity. This condition may be violated close to the intrusion, where the thermal front may induce large pressure gradients and where mechanical strains may be large [*Ylinen and Elsworth*, 1991]. However, since advection will more effectively distribute the zone of increased pressure over a wider area, the assumption of diffusive-only transport is expected to yield a lower pressure change than actual and hence give a conservative bound to stability. This conservatism is further manifest as induced pressures are limited to lithostatic magnitudes, as discussed later.

The solution is a one-dimensional heat flow model assuming the dike is emplaced instantaneously along the rear boundary of the failure block at time $t = 0$. Consequently, estimation of thermal effects at early times, of the order of dike emplacement durations ($t \approx d/U$), will be less reliable than at $t \gg d/U$ where the solution should offer a more truthful representation of thermal behavior.

The diffusion-induced pressure rise represented in equation (16) is also only appropriate for small magnitudes of the material parameters $A$ and $D$ [*Delaney*, 1982]. For the geological systems under consideration the ratio of diffusivities, $D$, is safely much less than unity. Magnitudes of thermally induced fluid expansion in the porous medium, as conditioned by the parameter $A$, are sufficiently large that the original assumptions engendered in equation (16) are violated. However, comparisons between a system including the full influence of large thermal expansions and the simplified representation of equation (16) suggest that the underprediction of pressure in the simplified system is less than 20% [*Delaney*, 1982]. Although this underprediction of pressure will result in an unconservative estimate of stability (i.e., the analysis predicts a more stable flank than reality), the magnitude of the underprediction is an absolute upper bound as lithostatic limits on maximum pore pressure magnitudes will temper this lack of conservatism. Correspondingly, the representations of thermally induced pore pressures described in the preceding are considered appropriate for a first-order estimate of behavior and are used with these limitations in mind.

Evaluating the integrated influence of temperature-induced fluid pressure rise, in dimensionless form, gives

$$\begin{aligned} d\int_0^\infty \frac{P_D^t}{\sqrt{4t_D z_D}} dz_D &= d\int_0^\infty \frac{1}{\sqrt{4t_D z_D}} \mathrm{erfc}\left(\frac{Dz_D}{t_D}\right) dz_D \\ &= \frac{d}{\sqrt{\pi}} \frac{1}{D\cos\alpha} \end{aligned} \tag{20}$$

where the $\cos\alpha$ term accounts for the inclination of the plane from the unit normal vector to the dike face. The resulting total fluid pressure is given as

$$F_{pt} = dAK_b \sqrt{\frac{4\kappa t}{\pi}} \frac{1}{\cos\alpha} \tag{21}$$

or in nondimensional form, by dividing through by $\gamma_w h_s^2$, this is modified to

$$\bar{F}_{pt} = \frac{d}{h_s}\frac{AK_b}{\gamma_w h_s}\frac{1}{\sqrt{\pi}}\sqrt{\frac{4\kappa t}{h_s^2}}\frac{1}{\cos\alpha} \tag{22}$$

to give the thermal influence. The ratio of thermal and hydraulic diffusivities of the medium, $D$, has no influence on the uplift force, $F_{pt}$, where the limits of integration of equation (20) are zero to infinity. However, the change of variables implicit in the transformation of equation (20) requires that the integration limits are functions both of geometry and $D$. Where the zone of thermally induced pore pressures is larger than the projected failure plane, the limits of integration include material parameters and the uplift pressure is also controlled by the ratio of diffusivities, $D$.

The thermal influence on the pore pressure may be conveniently represented in terms of dimensionless groupings of parameters,

$$F_{pt} = d_D A_D \sqrt{\frac{t_D}{\pi}}\frac{1}{D\cos\alpha} \tag{23}$$

with

$$A_D = \frac{AK_b D}{\gamma_w h_s} \tag{24}$$

where the new dimensionless group, $A_D$, represents the fluid volume generated by the temperature change.

The magnitudes of uplift forces developed in an infinite medium by the mechanical and thermal processes that accompany dike intrusion may be influenced by the actual semi-infinite geometry of the volcano flank. As discussed later, the calculated magnitudes of induced pore fluid pressure may require truncation.

## Slope Geometry

The induced pore pressure distribution that results from dike intrusion may be used to assess the stability of adjacent slopes. For the plane geometry chosen in this study, translational displacement of a single wedge is an appropriate mode of failure [*Dieterich,* 1988; *Iverson,* 1992, 1995]. This geometry is illustrated in Figure 3. The wedge is bounded at the rear by the planar dike, of height, $h_m$, and at the base by a potential failure plane of arbitrary inclination, $\alpha$. The slope geometry incorporates a sea level, at height $h_s$ below the apex of the slope and a groundwater surface climbing from sea level at an angle, $\theta$. The slope angle is defined as $\beta$ and the geometry is characterized by wedge width, $d$, as illustrated in Figure 4.

From knowledge of these geometric parameters it is possible to determine the magnitude of forces acting on the free-body of the wedge. The pressure applied to the wedge by the loading of the sea is assumed to vary linearly with depth and is given by the product of depth

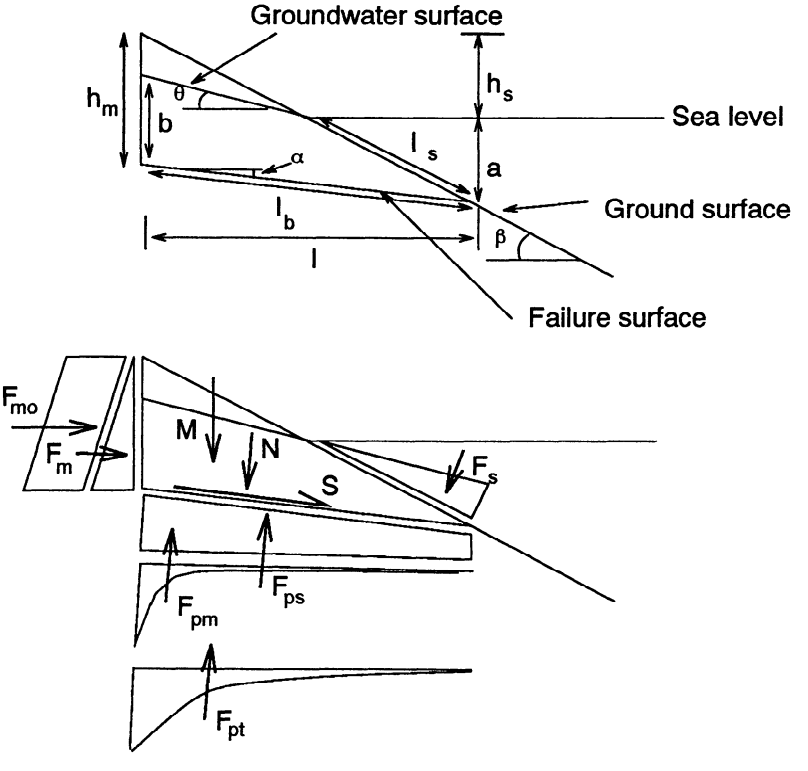


**Figure 3.** Generalized geometry for limit equilibrium analysis and identification of parameters. All quantities are defined as positive; $\alpha$ is defined positive for deep-seated failure and defined negative for long-runout failure. Forces acting on the system are block weight, $M$, seawater pressure, $F_s$, magma force, $F_m$, static groundwater force, $F_{p_s}$, and induced pore pressure forces that result from mechanical, $F_{p_m}$, and thermal, $F_{p_t}$, strains.

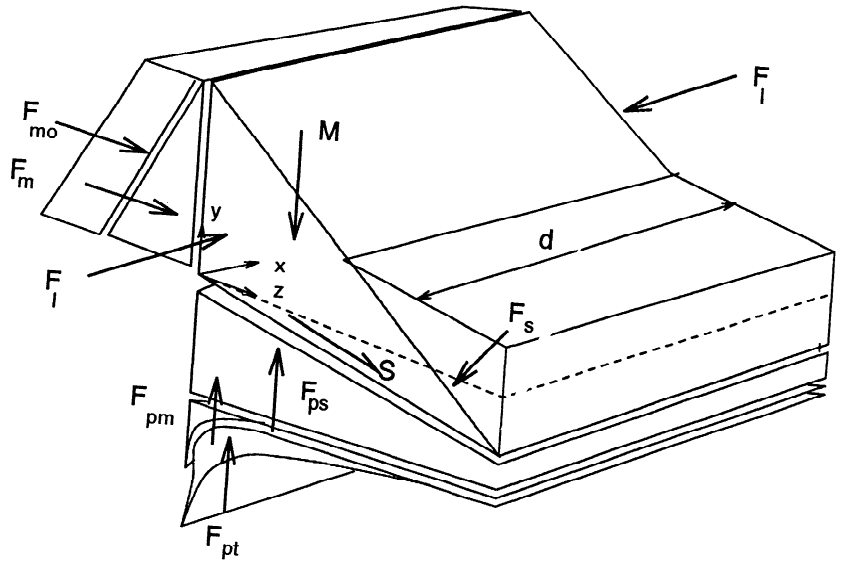


**Figure 4.** Perspective view of three-dimensional geometry illustrating forces, including lateral forces, $F_l$, and block width, $d$. The influence of lateral restraint in resisting failure is evaluated in terms of effective stresses. The proposed fluid pressure distribution is integrated over the triangular face of the block and subtracted from the integrated total stress. All lengths are as defined in the appendix.

below sea level and unit weight of water, $\gamma_w$. The total force acting normal to the submarine surface of the wedge is defined as $F_s$ and is given in the appendix. The uplift pressures acting on the base of the wedge are defined by the presumed hydrostatic heads acting at the dike contact and toe. These magnitudes are defined according to Figure 3 as $b\gamma_w$ and $a\gamma_w$, respectively, where the difference in unit weights of seawater and fresh water are considered negligible. A linear variation in uplift pressure is assumed to contribute to the static uplift force, $F_{ps}$. This is expected to be reasonable for inclined failure planes that outcrop (daylight) well below sea level but is less realistic for those that daylight at sea level. For those that daylight close to sea level, a parabolic distribution would be more representative of the pressure distribution. Choice of a parabolic distribution over a linear distribution will increase the potential uplift force by a maximum of one sixth for a base plane that daylights at sea level. This difference is considerably diminished for successively deeper failure surfaces. Thus a linear distribution is used, with the resulting calculation yielding a slightly higher factor of safety than would be returned for the parabolic distribution.

Since the analysis is defined in terms of effective stresses, the influence of lateral stresses in resisting failure must also be defined in terms of effective stress parameters. The total stresses acting on the block result from self-weight and surcharge by the seawater wedge. The assumed pore fluid pressure distribution incorporates the seawater effect at the toe and static groundwater conditions at the rear block scarp. These conditions are used to determine the magnitude of the lateral force, $F_l$, resulting from earth pressure at rest. For simplicity, intrusion-induced pore fluid pressures are not subtracted from the assumed total stress distribution. This simplification is conservative in the context of this analysis, since the slope will always be less stable in reality than predicted.

The average unit weight of the material comprising the failing wedge is defined as $\gamma_r$, enabling the mass, $M$, of the wedge to be determined from the previously defined geometry. For the purposes of this analysis the strength along the potential failure surface is assumed to be characterized by a single value of "apparent" friction angle, $\phi$. The actual frictional resistance will be stress level dependent, and cohesion may be important. These components must be averaged over the length of the basal failure plane. It is this aggregate value that is represented by the "apparent" frictional angle, $\phi$. The magnitudes of these forces are given in nondimensional form in the appendix.

For the planar dike, lateral magma pressure acting on the wedge is decomposed into two components. The first is the lateral pressure resulting from the static magma column, assumed to vary linearly with depth. The lateral force resulting from the static column, $F_{ms}$, is given as $F_{ms} = \frac{1}{2}h_m^2\gamma_m$, where $\gamma_m$ is the unit weight of magma. In addition to the hydrostatically generated pressures from the magma column, magma "overpressures" may exist to drive the magma conduit flow [*Rubin and Pollard,* 1987; *Iverson,* 1992, 1995]. Such magma overpressures influence flank stability through the application of an additional lateral force, $F_{mo}$, assumed constant with depth, and defined as $F_{mo} = h_m p_o$, or $F_{mo} = h_m h_o \gamma_m$, where $p_o$ is the magma overpressure and $h_o$ is the equivalent excess height of the magma column corresponding to the overpressure mag-

nitude. The latter definition is preferred as it avoids use of a pressure term that may be confused with excess pore pressures generated in the country rock. The resulting lateral force, $F_m$, is defined as the sum of the two components, $F_m = \zeta(F_{ms}+F_{mo})$, where the magma loading is applied over half of the rear block scarp for the mechanically induced pore pressures (Figure 1) as $\zeta = \frac{1}{2}$ and over the full block width for thermally induced pore pressures as $\zeta = 1$.

Pore pressures mechanically induced by the dike intrusion process are present along the base of the wedge and may be readily determined from the integral of equation (12). The magnitude of this uplift force, $F_{p_m}$, is given in the appendix, for the specific geometry of the wedge, using appropriate dimensionless parameters. Thermal pore pressure magnitudes are defined in the integrals of equation (20) and in the closed form solution of equation (22), again repeated in the appendix for completeness.

## Stability Analysis

For the geometry illustrated in Figure 3, resolution of forces parallel to the basal failure plane enables the total force driving outward wedge movement to be determined as $S$. This force is countered by the shear strength that is mobilized along the basal failure plane and along the sides of the wedge. The width of the failure block is defined as $d$. Correspondingly, the mobilized shear force, $S$, is defined purely in terms of the "apparent" frictional resistance, $\phi$, as

$$S = \frac{N \tan \phi}{F} \tag{25}$$

where $F$ is the factor of safety against failure and $N$ is the effective normal force acting perpendicular to the failure surface. The nondimensional factor of safety for the slope against failure is defined as

$$\frac{F}{\tan \phi} = \frac{N}{S} = \frac{\text{stabilizing forces}}{\text{destabilizing forces}} \times \frac{1}{\tan \phi} \tag{26}$$

where the normal, $N$, and shear, $S$, components acting on the basal plane, and on the sides of the failing block, may be resolved from Figures 3 and 4 (for simplicity the same frictional angle, $\phi$, is assigned to basal and lateral failure planes). Resolving the components normal and parallel to the failure plane, and resubstituting into equation (26) gives

$$\begin{aligned} F/\tan\phi \;=\; & [\bar{M}\cos\alpha + F_m \sin\alpha + \bar{F}_s \cos(\beta+\alpha) \\ & -\bar{F}_{p_m} - \bar{F}_{p_s} - \bar{F}_{p_t} + \bar{F}_l][-\bar{M}\sin\alpha \\ & +\bar{F}_m \cos\alpha - \bar{F}_s \sin(\beta+\alpha)]^{-1} \end{aligned} \tag{27}$$

where the overbar denotes the nondimensional magnitude of the forces. Forces acting on the wedge are made dimensionless by dividing throughout by $\gamma_w h_s^3$. $M$ is the weight of the failing block, $F_m$ is the composite lateral force generated by the combined magma column pressure and magma overpressure, $F_s$ is the "downward" force on the wedge resulting from loading by seawater, $F_{p_m}$ is the uplift force supplied by pore fluid pressures mechanically generated by dike intrusion, $F_{p_t}$ is the uplift force supplied by the thermal influence of the intruded dike, $F_{p_s}$ is the force resulting from the static groundwater pressure, and $F_l$ is the lateral force due to the effective lithostatic pressure. The lateral force resulting from lithostatic pressure is defined in terms of $k_0$, denoted as the coefficient of earth pressure at rest and given by the ratio of vertical effective stress to horizontal effective stress [*Lambe and Whitman*, 1979]. The distribution of solid body and pore fluid forces, acting on all sides of the failing block, is defined in Figure 4. Summarized magnitudes of all forces acting on the wedge are given in the appendix.

### Limiting Magnitudes of Pore Pressure

Where excess fluid pressures are developed by the mechanical or thermal processes that accompany dike intrusion, a sensible upper maximum pressure or resultant body force may be defined that is consistent with the magnitude of vertical lithostatic stresses. Although it is feasible that localized fluid pressures may exceed lithostatic, the admissible overpressure magnitude and the extent of the overpressured zone may be determined only by a more sophisticated, coupled analysis that includes poorly understood elastic and flexural attributes of the wedge. To retain the simplicity of the previous approach, two approximate methods may be used to limit the maximum magnitude of the induced uplift force or uplift pressure, respectively. Correspondingly, these limits are referred to as force and pressure controls on the destabilizing effect of the intrusion.

Limiting the maximum magnitude of uplift force to the buoyant weight of the sliding block is consistent with the assumptions of the limiting equilibrium analysis where the sliding block is assumed rigid. The mechanical and thermal uplift forces induced during intrusion may be determined directly from $\bar{F}_{p_m}$ and $\bar{F}_{p_t}$ in equations (10) and (22), respectively. These magnitudes are developed without concern for the presence of the free surface and may exceed the integrated lithostatic stresses distributed over the base of the wedge. To provide an upper bound for the magnitude of the mechanically induced uplift force, $\bar{F}_{p_{max}}$ is effectively limited by

$$\bar{F}_{p_{max}} = [\bar{M} - (\bar{F}_{p_s} + \bar{F}_{p_t})\cos\alpha + \bar{F}_s \cos\beta]\frac{1}{\cos\alpha} \tag{28}$$

where the terms in the brackets represent the buoyant mass of the failing block when only static water pressures are acting.

As an alternative to limiting the uplift force, the peak induced pressure may be locally truncated where it ex-

ceeds lithostatic stress. This pressure control considers the sliding block to exhibit no flexural rigidity and represents the behavior of a flexible rather than rigid sliding mass. Idealization of the system as a flexible block enables the pressure-limiting development of a shallow inclination hydraulic fracture adjacent to the intruding dike. This physical process will effectively limit local fluid pressures to lithostatic.

The pressure control mechanism is chosen as more realistic and is used in the following analyses. Where fluid pressures locally exceed lithostatic, the resulting integrals for maximum uplift must be evaluated numerically. Where the pressure criterion is applied, equation (28) is automatically satisfied. If, alternatively, the force criterion is applied, pore pressures may locally exceed lithostatic stresses.

## Controls on Stability

From equation (27), the minimum set of dimensionless coefficients that describe the stability of the isothermal system may be determined as

$$\frac{F}{\tan\phi} = f[\alpha,\ \beta,\ \theta,\ \frac{\gamma_m}{\gamma_w},\ \frac{\gamma_r}{\gamma_w},\ \frac{h_m}{h_s},\ \frac{d}{h_s},\ \frac{h_o}{h_s},\ k_0,\ w_D,\ \frac{Uh_s}{2c}]. \quad (29)$$

This is the minimum set of parameters that control the behavior of the system. In determining $F/\tan\phi$, the inclination of the basal plane, $\alpha$, could be optimized to determine the critical magnitude, $\alpha_c$, that defines the minimum factor of safety, $F$. However, if stratigraphy and structure present an overriding control on strength, as they generally do, preferential inclinations of the basal failure plane may be apparent. Selected inclinations of the failure plane that are compatible with the stratigraphy are used to provide an upper bound to the evaluated stability. Only an upper bound results, since failure modes that seem kinematically more critical are excluded by the overriding influence of weak layers. Consequently, where the interest is in conveying the potential for dike intrusion to trigger failure, this upper bound solution is most appropriate.

Additionally, the parameters $\beta$, $\theta$, $\gamma_m/\gamma_w$, $\gamma_r/\gamma_w$, and $k_0$, are known within relatively well defined limits for any particular example and may usually be defined with some confidence. Eight primary variables remain that control behavior. Two represent the variable geometry of failure through $h_m/h_s$, and $d/h_s$, to define the depth and width of the failure plane, respectively. The mechanical influence of the dike is represented through the dimensionless dike width, $w_D$, and the dimensionless dike propagation rate, $U_D$. Where thermal effects are included, the system is additionally controlled by the dimensionless groupings of parameters

$$\frac{\kappa n}{c},\ \frac{4\kappa t}{h_s^2},\ \frac{AK_bD}{\gamma_w h_s} \quad (30)$$

representing the ratio of thermal and hydraulic diffusivities, $D$, dimensionless time, $t_D$, and magnitude of the thermal forcing, $A_D$, respectively (see equations (18), (19) and (24)). Finally, where the influence of magma overpressure is added to the system, the additional variable representing excess magma column height, $h_o/h_s$, must also be accommodated.

## Flank Slip Runout

The previous analysis describes only the potential to initiate failure and provides no insight into the ability of the system to sustain failure, as required in a runout slide. Sustainable failure requires that the ratio of stabilizing to disturbing forces remains less than unity following initial failure. The stabilizing components act directly on the shear resistance, $\phi$, of the basal and lateral rupture planes. First, residual strengths of both indurated and nonindurated rocks are commonly lower than peak strengths mobilized at failure. Once failure is initiated, this strength drop may be sufficient to sustain failure. Second, significant excess pore pressures, $\Delta p$, may be developed. These may be quantified in terms of stress changes where the stress tensor is decomposed into independent components that represent changes in the 'mean' stress, $\Delta\sigma_3$, and 'deviatoric' stress, $\Delta\sigma_1 - \Delta\sigma_3$, namely, $\Delta p = B\Delta\sigma_3 + A_f(\Delta\sigma_1 - \Delta\sigma_3)$ [*Skempton,* 1954]. $B$ is typically close to unity for fine-grained sediments and claystones and decreases toward 0.3 with increasing matrix stiffness or permeability [*Lambe and Whitman,* 1979]. The $A_f$ parameter is not a constant material property but depends on state of stress, stress history, total strain, and other factors. $A_f$ varies with the sensitivity of the material, being one third for an elastic material and typically $0 < A_f < 1$ at failure for a variety of geologic materials. Loose, unstable materials such as tephra may yield $A_f > 1$ [*Voight and Sousa,* 1994]. Dense granular materials and fractured rocks that dilate with rupture may yield negative magnitudes of $A_f$ [*Goodman and Ohnishi,* 1973]. For sensitive materials, however, the overriding influence is likely a reduction in strength, increase in pore pressure, and a corresponding reduction in restoring force. Similarly, pore pressure enhancement may occur as a consequence of frictional heat released during shear [*Voight and Faust,* 1982], and of dynamic rapid shear of saturated granualar debris [*Iverson and LaHusen,* 1989].

If the slide toe moves over marine sediments covering the submarine portion of the volcano flank, undrained loading of these "unstable" sediments is likely to result in a profound drop in shear resistance [*Voight and Elsworth,* 1992; *cf. Hutchinson and Bhandari,* 1971; *Sassa,* 1988; *Voight and Sousa,* 1994]. With further displacement, progressively more of the shear resistance of the displacing block is borne on these weak sediments, and an accelerating instability may result. As speed increases, hydrodynamic drag augments the resisting force and places limits on acceleration, velocity, and runout.

The components of forces driving flank failure are represented in the denominator of equation (27). The influence of slide mass, $M$, and forces due to sea level, $F_s$, do not change substantially under limited movement of the block. Magma pressure will dissipate with significant displacement of the wedge.

Although the above mechanisms are not quantified here, the conclusion remains that under appropriate conditions they are sufficient to sustain failure, provided flank rupture is initiated. Therefore large postfailure displacements are not regarded as truly enigmatic, and the record of prodigious, long-runout submarine landslides [*Moore,* 1964; *Moore et al.,* 1989] may indeed be largely explained on the basis of failure initiation, as primarily considered in the following.

## Relevance to Oceanic Shield Volcanoes

Shield volcanoes of the Hawaiian type are emphasized here. Seventeen gigantic mass movements were first identified from Kauai to Hawaii [*Moore et al.,* 1989], and subsequent surveys discerned about 40 more along the Emperor Seamount Chain from Kure Island to Kauai [*Holcomb and Searle,* 1993]. Similar phenomena are known from the Indian Ocean at Réunion Island [*Duffield et al.* 1982; *Lénat et al.,* 1989; *Labazuy and Lénat,* 1990] and at Tristan da Cunha and the Canary Islands in the Atlantic [*Holcomb and Searle,* 1993]. Arcuate margined atolls, often with corresponding bulging submarine contours, probably also reflect submarine landslides and are reported from the Central Pacific in the Makin, Kuria, Aranuka, Gilberts, Carolines, and Marshalls, as well as from stratovolcanoes in the Banda Sea [*Fairbridge,* 1950]. In order to examine the generic influence of dike intrusion on the stability of volcano flanks, two separate models for failure are selected, namely, shallow and deep-seated failure, corresponding to the two major types of mass movements recognized in submarine surveys. The shallow failure model is characterized by a failure plane sloping in the same direction as the volcano flank and offers the potential of producing rapid, long runout landslides of the "debris avalanche" type evident in the bathymetric record [*Moore et al.,* 1989]. Moreover, the term "shallow" is used in a relative sense, in comparison with the dimensions of the volcano edifice. Such shallow slides may produce prodigious mass movements, involving volumes as great as 5000 km$^3$ and reaching more than 200 km from their source. The model representing deep-seated "slump" failure comprises a deep basal failure plane, relatively flat and possibly dipping in the opposite direction to the overlying flank. It is postulated that deep-seated failure may cause rapid but limited displacement and may augment the earthquake record but, due to the geometry of the basal plane, is unlikely to be capable of sustaining a rapid long-runout failure.

Typical structure of an oceanic volcano is shown in Figure 5. P-wave velocity structure of the volcano

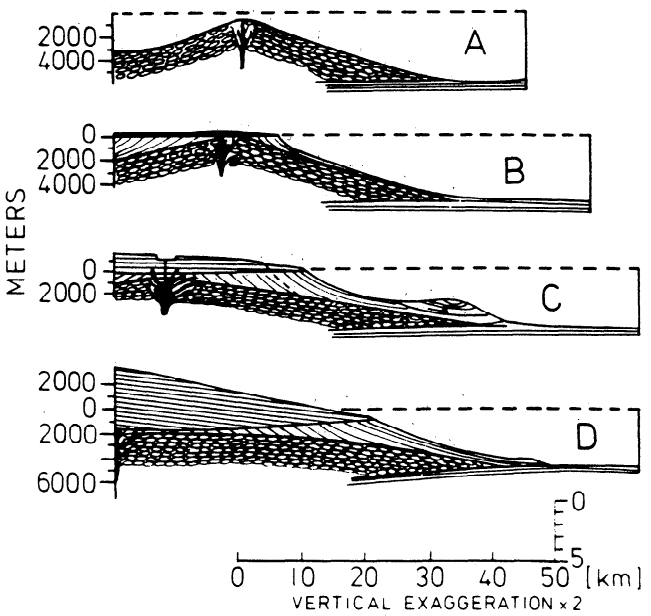


**Figure 5.** Cross sections illustrating oceanic volcanic islands in submarine, sea level, and subaerial stages of evolution (reproduced from *Moore and Fiske* [1969]). Patterns indicate rock types: ovals, pillow lavas with included pillow fragments and sediment; lined pattern, clastic rocks, including phreatic explosion ash, littoral cone ash, and flow foot breccia and including some pillowed flows and pillowed breccias; dark pattern, subaerial lava flows with minor ash; solid black, intrusive rock. Note contrast between submarine and subaerial slopes, continuation of clastic layer beneath subaerial shield, and downbowing of seafloor by subsidence caused by volcanic loading. Dike swarm may occur deep within the edifice, overprinted on pillow lavas.

flanks supports the *Moore and Fiske* [1969] model for the volcanic pile, in which an inner wedge of submarine pillow basalt (and intrusives) is covered by a mantle of hyaloclastics and subaerial basalt flows [*Hill and Zucca,* 1987]. Material parameters relevant to both forms of analyses are included in Table 1, together with a complete listing of sources. The enveloping geometry chosen in all of the analyses is of a flank rising at an angle, $\beta$, of 10° from the seafloor with the static groundwater surface rising from sea level at an angle, $\theta$ of 2°. Although estimates of frictional resistance, $\phi$, are reported in Table 1, the results of the analyses are reported through the normalized quantity $F/\tan\phi$ and are therefore not confined to the estimates provided. At the initiation of failure, $F \rightarrow 1$ and values of $F/\tan\phi$ are of the order 1.9 to 1.2 for friction angles, $\phi$, of 28° and 40°, respectively.

### Shallow Flank Failure

Where shallow failure of the flank is considered in the absence of mechanically or thermally induced pore pressures but in the presence of a hydrostatic force from the magma, $F_m$, stability is conditioned only by lateral restraint, width of the failing block, and depth and

**Table 1.** Material Parameters Selected as Representative of the Mechanical and Thermal Properties of Volcano Flanks

| Parameter (Reference) | Magnitude |
|---|---|
| Slope height above sea level $h_s$ | 1000 m |
| Shear modulus $G$ (1) | $3 \times 10^3$ MPa |
| Poisson ratio $\nu$ (2) | 0.22 – 0.28 |
| Frictional resistance $\phi^*$ | 20° – 60° |
| Coefficient of earth pressure at rest $k_0$ (3) | 0.5 |
| Unit weights | |
| Water $\gamma_w$ | $10 \times 10^{-3}$ MPa/m |
| Rock $\gamma_r$ (4) | $23 - 29 \times 10^{-3}$ MPa/m |
| Magma $\gamma_m$ (5) | $26 - 28 \times 10^{-3}$ MPa/m |
| Volcaniclastic debris† | |
| Permeability $k/\mu$ (6) | $1 - 2 \times 10^{-11}$ m²/Pa.s |
| Hydraulic diffusivity $c$ (6) | 770 – 1550 m²/s |
| Intrusion width $w$ (7) | 1 ($1 \times 10^{-3}$)‡ m |
| Intrusion rate $U$ (8) | 0.27 – 0.75 m/s |
| Fractured lava † | |
| Permeability $k/\mu$ (9) | $1.65 - 7.2 \times 10^{-6}$ m²/Pa.s |
| Hydraulic diffusivity $c$ | $1.5 - 6.5 \times 10^{6}$§ m²/s |
| Intrusion width $w$ (10) | 1 m |
| Intrusion rate $U$ (11) | 0.1-0.5 m/s |
| Thermal parameters | |
| Thermal strain $A$ (12) | 0.9 – 1 |
| Skeletal modulus $K_b$ (12) | $0.4 - 1.2 \times 10^3$ MPa |
| Thermal diffusivity $\kappa$ (12) | $10^{-6}$ m²/s |
| Porosity $n$ (12) | 0.05 – 0.2 |

References: 1, *Davis* cited by *Rubin and Pollard* [1987]; 2, *Rubin and Pollard* [1987]; 3, estimated from *Dieterich* [1988]; 4, *Zucca and Hill* [1980]; *Zucca et al.* [1982]; *Rubin and Pollard* [1987]; 5, *Decker* [1987]; 6, *Sigurdsson* [1982]; *Bodvarsson et al.* [1984]; 7, *Tryggvason* [1980]; *Elsworth and Voight* [1992]; 8, *Brandsdottir and Einarsson* [1979]; *Elsworth and Voight* [1992]; 9, *Thomas* [1987]; *Mink and Lau* [1980]; 10, *Delaney and Pollard* [1981]; *Rubin and Pollard* [1987]; 11, *Delaney and Pollard* [1981]; 12, *Delaney* [1982].

* Possibly $\phi$ may be close to, or lower than, the lower limit of the range where clays dominate the key stratigraphic horizon, but it is questionable whether these low values are appropriate for the entire basal failure plane, including subacrial and submarine parts. Lower range values are representative of clays and mudstones. Upper range values are representative of angular granular debris or weak rock, and include the effect of cohesion on apparent friction angle.

† Volcaniclastic data are based on studies at Krafla volcano by authors cited; lava data are based on studies in the Hawaiian Islands by authors cited.

‡ Unbracketed value represents observed thickness. Bracketed value represents thickness estimate consistent with parameters used in the evaluation of intrusion-induced fluid pressures. See discussion in text.

§ Magnitude of hydraulic diffusivity is estimated from $c = 2(k/\mu)G(1-\nu)/(1-2\nu)$ to give representative value for incompressible fluid and grains [*Rice and Cleary*, 1976]. Parameter range obtained through using $\nu = 0.25$, and shear modulus $G$ and permeability $k/\mu$ ranges defined in the table.

angle of the basal failure plane. All other parameters are constrained by the assumed geometry and by the narrow ranges of variability of the density parameters, defined in Tables 1 and 2. The geometry of the system sensibly constrains the dip of the failure surface to $0° \geq \alpha \geq -10°$, with a critical inclination of $\alpha_c = -6°$ evaluated for large dimensionless widths, $d_D$. Using this critical magnitude of failure plane inclination, stability is evaluated for different magnitudes of lateral earth pressure coefficient, $k_0$, and depth of failure, $h_m/h_s$, as recorded in Figure 6. Where the effects of lateral restraint are discounted ($k_0 \rightarrow 0$), it is apparent that very shallow failure (say $h_m/h_s = 1$) is easiest to initiate due to the diminished influence of the stabilizing force due to loading by seawater, $F_s$. At increasing depth this stabilizing influence increases faster than the buildup in driving force from the magma. Consequently, in the ensuing evaluation of shallow flank stability, $h_m/h_s = 1$ is selected as a suitable representative value.

The relative influence of lateral restraint decreases as dimensionless block width, $d_D = d/h_s$, increases. For an increasing depth of failure, an increased failure width is necessary to enable the problem to be characterized in two-dimensional rather than three-dimensional form. For $h_m/h_s = 10$ the required width becomes prohibitive, even for relatively modest values of $k_0$ as evidenced in Figure 6. For shallower systems ($h_m/h_s = 1$), the definition of $k_0$ is less critical (Figure 6). In the geologically young and predominantly gravity-loaded environment characteristic of volcanic rift zones, sublithostatic magnitudes of lateral stresses are generally expected [*Rubin and Pollard*, 1987; *Dieterich*, 1988], and $k_0 = 0.5$ is presumed reasonable. In the absence of an initiating mechanism, and with nominal values of frictional resistance, $\phi$, the representative wedge char-

**Table 2.** Dimensionless Parameters Used in the Evaluation of Mechanically Induced Pore Pressures

| Dimensionless Grouping | Parameter Range | Reference |
|---|---|---|
| $\gamma_m/\gamma_w$ | 2.6 | |
| $\gamma_r/\gamma_w$ | 2.3 | |
| Volcaniclastic debris | | |
| $w_D^*$ | $2.5 - 30 \times 10^2$ | 1 |
| | $0.25 - 4 \times 10^6$ | 2 |
| $U_D^\dagger$ | 0.1 – 1 | |
| Fractured lava | | |
| $w_D^*$ | $1 - 1 \times 10^{-3}$ | |
| $U_D^\dagger$ | $0.4 - 1.7 \times 10^{-4}$ | |

Dimensionless parameters of width, $w_D$, and intrusion velocity, $U_D$, are defined in equations (7) and (3), respectively.

References: 1, *Elsworth and Voight* [1992]; 2, *Tryggvason* [1980] and *Delaney and Pollard* [1981].

* Magnitude of $w_D$ is estimated from the material coefficients and geometric parameters of Table 1. The upper bound magnitude is representative of a 1-m-wide dike, and the lower bound is for a $10^{-3}$-m-wide dike consistent with the parameter evaluations of *Elsworth and Voight* [1992].

† Estimate uses permeability and hydraulic diffusivity parameters for the two volcanic environments, with other data from Table 1. An intrusion velocity of 0.5 m/s is considered representative of both Icelandic and Hawaiian eruptions.

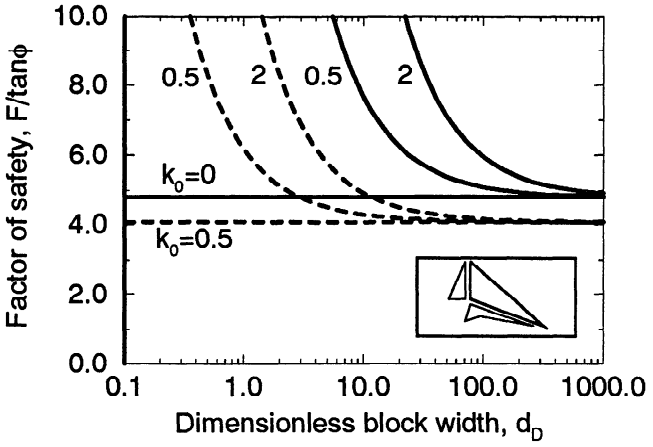


**Figure 6.** Variation of normalized factor of safety for a long-runout failure of a volcano flank in the initial condition. Results are for the critical failure plane inclination of $\alpha_c = -6°$ and for contrasting failure heights, $h_m/h_s$, of 1 (dashed) and 10 (solid). Behavior for variable values of coefficient of earth pressure at rest, $k_0$, is shown.

acterized by the evaluations of Figure 6 is anticipated to remain stable.

**Mechanical influence.** Where the influence of mechanically induced pore fluid pressures is added to the static behavior illustrated in Figure 6, the two additional parameters of dimensionless intrusion rate, $U_D$, and dimensionless dike width, $w_D$, (see equations (3) and (7)) exert added control on behavior. Field test based estimates of permeability and hydraulic diffusivity are provided for two representative materials: compact, partly altered basaltic volcaniclastic debris and fractured, weathered basaltic lava (Table 1). For the specific slope geometry of Hawaii, dimensionless intrusion rates, $U_D$, are in the range $10^{-4}$ to $10^0$.

The dimensionless rate of intrusion influences the morphology of the pressure bulb that develops around the advancing dike front [*Elsworth,* 1991]. As $U_D$ increases to and beyond $10^0$, the pressure bulb becomes elongated along the path of propagation ($x$ axis; see Figure 1). For magnitudes of $U_D$ less than $10^0$ the resulting pressure bulb is no longer elongate but exhibits a circular section in the $x - z$ plane. Since the intrusion rates anticipated for this system straddle the boundary between these two different forms of behavior, both effects are manifest in the stability response. The relevance of this observation, with regard to stability, is that dimensionless intrusion rates more rapid than $10^0$ result in an induced pressure distribution more tightly constrained close to the dike location. Slower propagation results in a more widespread distribution of pore fluid pressures over the failure plane, albeit of lower absolute pressure magnitude, and consequently exerts a more widespread and enduring influence on runout stability.

Dike propagation rate primarily influences the distribution of induced pore pressures, and dike width, reflected through $w_D$, controls the absolute magnitude of induced pressures. In the original matching of induced pressures observed at Krafla volcano with the model presented in equation (1), the surprisingly low estimate of $w = 10^{-3}$ m was returned for dike width where observational evidence suggested the width to be of the order of 1 m. This discrepancy occurred despite satisfactory estimates of the other evaluated parameters of propagation rate, $U$, and dike location. Where the same techniques are used to characterize the form of hydrofractures created in the stimulation of petroleum reservoirs, a similar underestimation of the fracture volume results [*Elsworth and Piggott,* 1992]. The disagreement between the "evaluated" volume and real "volume" apparently results from the influence of the free surface that is not accounted for in the solution for a dislocation in an infinite medium [*Ouyang,* 1994]. The effect of the free surface is to dampen the magnitude of the induced pore pressure response. This effect becomes more acute as the dike approaches the free surface, as is the case in the Krafla data set. The dichotomy may be resolved by using a range of parametrically consistent values of material parameters. Thus values in the range $10^{-1} \leq U_D \leq 10^0$ and $10^2 \leq w_D \leq 10^6$ are selected for volcaniclastic material, and $U_D = 10^{-4}$ and $10^{-3} \leq w_D \leq 10^0$ are selected for rock-mass lava, to compare trends in behavior. These values are summarized in Table 2 and their influence on stability of shallow flank failures is evaluated in Figure 7.

Figures 7a and 7b represent behavior consistent with volcaniclastic failure zone materials. For the upper bound of $U_D = 10^0$, as represented in Figure 7a, a variety of trends is apparent. For very small dike widths ($w_D \leq 10^{-1}$) there is no influence of mechanically induced pore fluid pressures, and the trend in decreased stability with increased width follows directly. As dike width is increased above $10^1$, the influence of mechanically induced pore fluid pressures monotonically increases. For narrow blocks, the stabilizing effect of lateral restraint dominates behavior. For large magnitudes of dike width, say $w_D = 10^6$, the stability curve exhibits three distinct zones, separated by cusps. The first zone is for dimensionless block width $d_D \leq 10^1$ and illustrates the rapidly diminishing influence of lateral restraint with increased block width. For this large magnitude of $U_D$ the induced pressure distribution is elongate and the mechanically induced uplift force, $\bar{F}_{p_m}$ increases in direct proportion to width. Thus for small block widths, $d_D < 10^1$, the pressure distribution is effectively identical in all parallel sections in the $y - z$ plane (the plane of cross section; see Figure 1), but for a second zone delimited by $10^1 \leq d_D \leq 2 \times 10^2$ an increase in stability occurs gradually with increased width. This rate of gain in stability is reduced as the width approaches the upper limit of the range in width. In this zone the uplift force increases less quickly than width as the ends of the elongate pressure distribution are felt inside the expanding area of the failure plane. This is especially pronounced for $U_D > 10^0$ where the

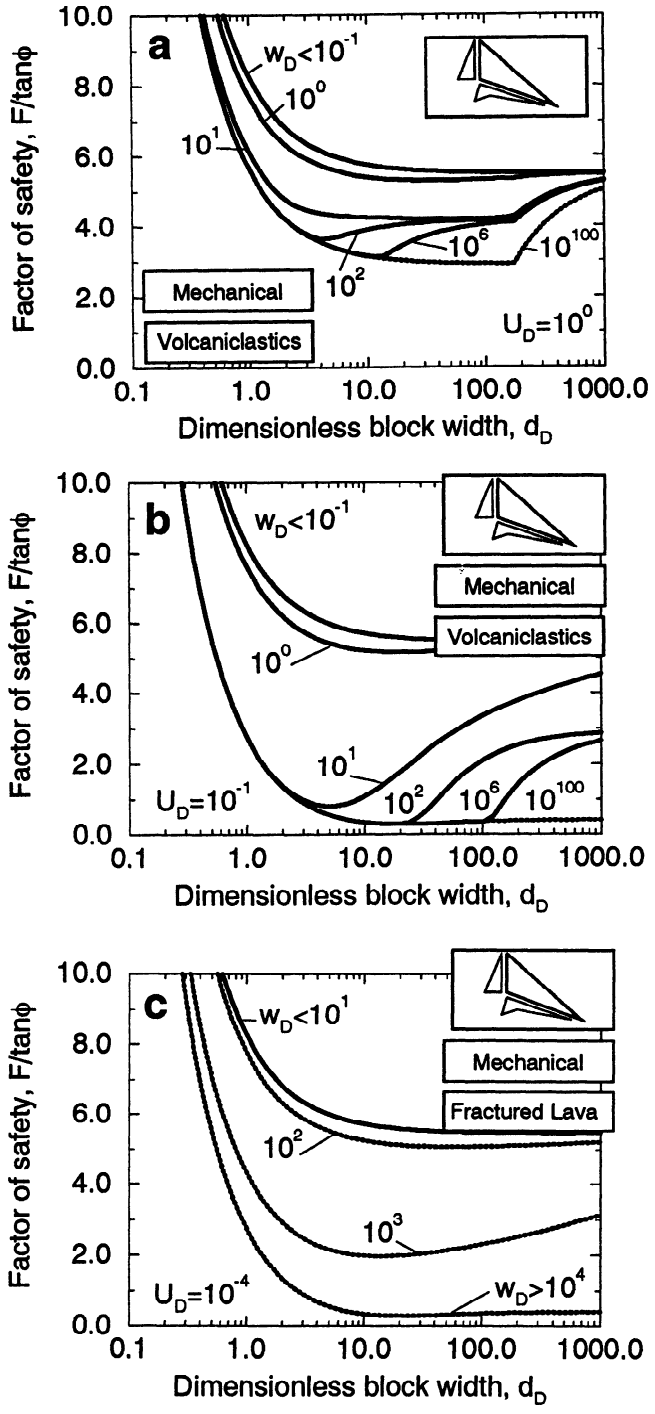


**Figure 7.** Variation of normalized factor of safety for a shallow long runout failure of a volcano flank with mechanically induced pressures resulting from dike intrusion for (a) $U_D = 10^0$, (b) $U_D = 10^{-1}$, and (c) $U_D = 10^{-4}$. Basal failure plane is inclined at $\alpha = -6°$, and $h_m/h_s = 1$. The observed range of dimensionless dike widths are shown (lined) together with larger than observed (dotted).

center of the pressure of the pressure distribution lags behind the advancing dike front [*Elsworth*, 1991]. Consequently, the uplift force increases at about half the rate of increase in dimensionless block width, $d_D$, as the true three-dimensional nature of the distribution becomes apparent between the limits of integration. The third zone is for $d_D \geq 2 \times 10^2$ and represents constant uplift force, $F_{p_m}$, as width increases. At these widths the pressure pulse is entirely contained within the lateral extent of the failure plane, and its relative influence diminishes as $d_D \rightarrow \infty$.

Of importance in defining the anticipated stability of these systems for volcaniclastic debris is to note the presence of a minimum stability for $w_D$ in the range $10^2$ to $10^6$. For values of $F/\tan\phi$ approaching 2 the slopes may be approaching the initiation of failure (i.e., for $\phi = 27°$, $\tan\phi \approx 0.5$ and $F/\tan\phi \approx 2$, and consequently, $F = 2. \times 0.5 \approx 1.0$; by definition, at failure, $F = 1$). The range in failure widths at these minima are $d_D$ of the order of $2 - 10$, representing $d = 2 - 10$ km for the selected geometry with $h_s = 1$ km.

As dimensionless dike propagation rate is decreased to $U_D = 10^{-1}$, representing a propagation rate of $10^{-1}$m/s (if hydraulic diffusivity is held constant), the stability of the system is substantially reduced, even for moderate values of dike width. This behavior is illustrated in Figure 7b. Similar trends in behavior are evident as for the "faster" intrusion, although minimum factors of safety are greatly diminished. Mechanically induced pore pressures appear sufficient to trigger failure to widths of the order of 100 km.

If material parameters possibly representative of fractured basaltic lava are utilized in the analysis, the results plotted in Figure 7c ensue. For representative magnitudes of $w_D$ in the range $10^0 - 10^{-3}$ the influence of mechanically induced pore fluid pressures appears insignificant. Thus for this mechanism, failure in volcaniclastic materials appears plausible, but failure in fractured lavas does not.

In addition to the application of hydrostatic disturbing forces applied through the magma column, additional overpressurization may be anticipated [*Rubin and Pollard*, 1987]; however, these effects are short lived and difficult to maintain at pressures appreciably above magmastatic (A.M. Rubin, personal communication, 1994). Correspondingly, the effects of overpressurization are neglected, and the magmastatic case is considered as a reasonable near upper bound for the magnitude of the downslope driving force.

**Thermal influence.** Concurrent with the mechanical generation of pore pressures, thermal strains and thermally driven groundwater flow will generate and spread additional excess fluid pressures. These mechanical and thermal mechanisms are additive, although the occurrence of maximum influence from each of the mechanisms is unlikely to coincide in time. Consequently, thermal influence is examined in isolation from mechanical effects, not merely as an analytical construct, but also as a plausible interpretation of reality.

Using the thermal parameters defined in Table 1 the appropriate ranges for the dimensionless parameters of thermal forcing, $A_D$, diffusivity ratios, $D$, and time, $t_D$, are determined, as summarized in Table 3. Param-

**Table 3.** Dimensionless Parameters Used in the Evaluation of Thermally Induced Pore Pressures

| Dimensionless Grouping | Parameter Range |
|---|---|
| $A_D^*$ | $24. - 0.008$ |
| $D$ | $0.2 \times 10^{-3} - 200. \times 10^{-3}$ |
| $t_D$ | $0.014,\ 1.4,\ 144. \times 10^{-6}$† |

* The broad parameter range of $A_D$ is conditioned mainly by the variability of hydraulic diffusivity, as represented in the ratio of thermal and hydraulic diffusivities $D$. Change in thermal forcing anticipated at depth is reflected through the parameter $A = \alpha\Delta T$ (see equation (24) and Table 1) that remains relatively insensitive to the magnitude of temperature increase.

† Dimensionless times represent dimensional times of 1 hour, 4 days, and 400 days.

eters are selected to represent expected ranges of block depth used in the subsequent stability analyses and are of the order of 1 to 10 km. The magnitude of thermal volume change, $A$, resulting from a prescribed temperature boundary condition is relatively insensitive to the choice of depth or thermal jump magnitude [*Delaney*, 1982](Table 3). The parameter with the widest natural variability in the constants $A_D$ and $D$ remains the ratio of thermal to hydraulic diffusivities, $D$, representing a material property rather than the magnitude of the thermal forcing. Consequently, the parameter ranges illustrated in Table 3 are considered representative of the full range of block depths later examined. The timescale of interest is chosen to span 4 orders of magnitude, with representative values 1 hour, 4 days, and an upperbound of approximately 1 year (400 days). For the parametric groupings representing the least destabilizing thermal effect, the influence on stability is barely discernible, as illustrated in Figure 8.

Conversely, the selection of maximum thermal forcing has a profound influence on stability. For this choice of parameters, the thermally induced pore pressures are sufficient to aid failure in time periods of the order of a week to a year. This scenario requires that the continuous temperature boundary condition at the dike face is maintained by a replenished supply of fresh magma over periods of this same order. This condition is consistent with a feeder dike but not with a "blind" dike that fails to reach the surface or one that is active only for a brief period. The sustained discharge (over months) of water in 1973 from a deep drill hole about 2 km from an erupting fissure at Heimaey probably reflects this mechanism [*Björnsson et al.*, 1977], although the geometry of the thermal source may have become localized over time.

Under these conditions, thermal straining of the host rock appears to be a viable agent to raise pore pressures and to aid flank failure in zones of weak materials. The ensuing displacements may result in significant changes in the driving forces acting on the wedge, and unless the induced basal pore pressures are sufficiently large to maintain the instability, failure will arrest. A limiting case for flank stability is included in Figure 8 where the driving magma force is removed; here the factor of safety relates to the period after the initiation of movement, and its low value illustrates the potential of this mechanism to sustain failure.

## Deep-Seated Flank Failure

The potential to develop deep-seated failure as a result of dike intrusion may also be examined through use of the block geometry defined previously. The geometry of the block incorporates a basal failure plane that rises from the rear dike scarp toward the slope toe. A potential basal failure plane is constrained to follow the updip attitude of the volcanic edifice, at depth, transformed from an initial subhorizontal orientation through subsidence driven by self-weight (Figure 5). Basal failure may involve the marine sediments under the volcanic pile in addition to the volcanic materials. Correspondingly, a basal inclination of $\alpha = +6°$ is used to represent the potential for failure at depth. Limited slip may occur with this failure plane orientation, and slip may be accompanied by an earthquake of significant magnitude; however, sustainable long runout is unlikely to occur.

**Mechanical influence.** The stability of a wedge with an updip basal plane is evaluated using dimensionless intrusion rates, $U_D$, and dike thicknesses, $w_D$, representative of the materials investigated earlier. Stability is evaluated for block depths, $h_m/h_s$, ranging be-

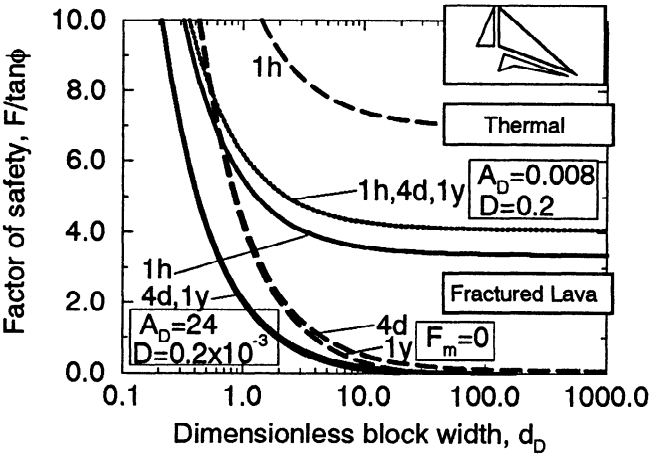


**Figure 8.** Variation of normalized factor of safety for a shallow long-runout failure of a volcano flank with thermally induced pressures resulting from dike intrusion. Analysis includes the disturbing influence of the magma column with results for the maximum thermal effect ($A_D = 24,\ D = 0.2 \times 10^{-3}$)(solid) and the minimum thermal effect ($A_D = 0.008,\ D = 0.2 \times 10^{-3}$)(dotted). Basal failure plane is inclined at $\alpha = -6°$. Also included is the variation of factor of safety with width where the magma driving force is removed following the initiation of block movement (long-dashed curves).

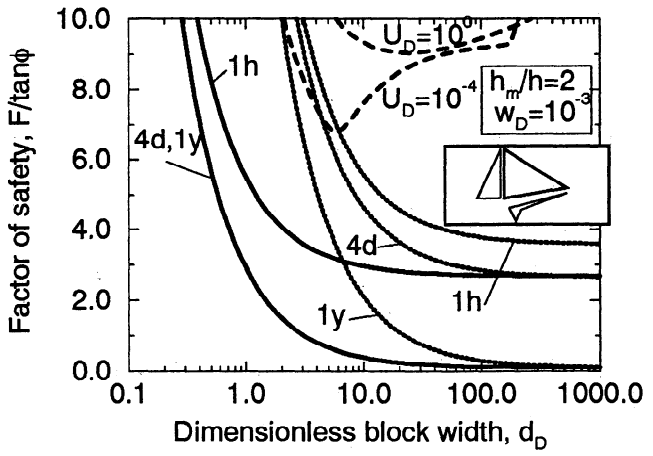


**Figure 9.** Variation of normalized factor of safety for a deep-seated failure of a volcano flank with mechanically and thermally induced pressures resulting from dike intrusion. Analysis includes the disturbing influence of the magma column. Mechanical results (dotted) are for $h_m/h_s = 2$ with $U_D = 10^0$ to $10^{-4}$ and $w_D = 10^{-3}$. Thermal results are for different magnitudes of the block rear scarp depth of $h_m/h_s = 2$ (solid) and $h_m/h_s = 10$ (dotted) for the maximum thermal effect with $A_D = 24$ and $D = 0.2 \times 10^{-3}$. Basal failure plane is inclined at $\alpha = +6°$.

tween 2 and 20, and for a full range of block widths, $d_D$, as illustrated in Figure 9. The mechanically induced excess pore pressures have the greatest destabilizing influence for the condition of shallowest overburden. Generally, deep-seated failure would not result except close to the intrusion where induced fluid pressures may locally exceed lithostatic. In this instance the limit equilibrium stability analysis is particularly conservative in representing localized instability, since induced excess pore pressures are aggregated over the entire failure surface rather than over the active portion of that surface. For the development of earthquake instability it is only necessary that effective stresses close to the dike intrusion are sufficiently reduced; thus local earthquakes may occur without concomitant slip on the full basal surface of the wedge. The general increase in rate of earthquakes following dike intrusion demonstrates that large portions of the volcano adjacent to the rift zones are near the point of failure and that forces induced by dike emplacement cause deformation of the volcano flank [*Koyanagi et al.*, 1972; *Swanson et al.*, 1976].

**Thermal influence.** The potential to generate deep-seated failure as the result of thermally induced pore fluid pressures is also illustrated in Figure 9. Thermal parameters selected are the end-members of the ranges defined in Table 3, i.e., those expected to yield the maximum effect. Particularly, if a feeder dike is sustained over a period of weeks to months, then the generation of deep-seated instability may be plausible, as implied from Figure 9. The distribution of induced fluid pressures along the basal failure plane is more evenly spread than for the corresponding case of mechanically induced pressures. Local instabilities would be anticipated close to the thermal source, with the corresponding potential for pressure dissipation resulting from rupture and dilation. The results of this behavior would be apparent, at depth, within the earthquake record.

Significant seismic energy may be released in association with such large-scale slip events triggered by dike intrusion [*Ando*, 1979], resulting in a destabilizing influence involving lateral accelerations that may affect other, shallower portions of the flank. Furthermore, the magnitude of the seismic energy release and its associated destabilizing influence may be enhanced by mechanically and thermally induced pore pressure mechanisms. Thus these mechanisms may play a potentially significant role in earthquake seismology.

## Seismic Influence

As discussed above, the potential to develop earthquakes of significant magnitude may be a natural consequence of intrusion, involving both magmatic driving forces and pore fluid pressurization mechanisms. Where pore fluid pressurization mechanisms are activated, the resulting seismic energy release may be orders of magnitude larger than that potentially released for the similar case with magmatic driving forces but lacking pore pressure enhancement. The effects of seismicity induced in this manner are manifest both in the potential reduction in shear resistance in adjacent materials subject to fluid pressurization and perhaps liquefaction, and also through the destabilizing influence of strong motions. The Hilina fault system in Hawaii [cf. *Stearns and Macdonald*, 1946; *Moore and Krivoy*, 1964] may be interpreted as the headwall of a large gravity slump episodically destabilized by seismic ground motion; in this case the earthquakes may be caused by forceful magma intrusion, and the slump is a secondary surficial feature only indirectly related to dike intrusion.

Earthquake forces are clearly capable over large regions of augmenting the load driving a potential slide mass [*Pariseau and Voight*, 1979; *Voight et al.*, 1983; *Keefer*, 1984]. Quantitative evaluations of stability include analyses requiring detailed time history of acceleration records and properties of materials (typically nonlinear and hysteretic) under dynamic loading [cf. *Newmark*, 1965; *Ambraseys and Sarma*, 1967; *Seed et al.*, 1969; *Seed*, 1981]. The alternative and standard procedure is the pseudostatic method [*Terzaghi*, 1950; *Seed*, 1979], which despite some limitations offers a simple and adequate means to evaluate the sensitivity of slope behavior to seismic loading.

Here the stability of both shallow and deep seated failures is examined for slopes subjected to a uniformly distributed effective lateral acceleration, $\delta$, of the order of $0.1g$ to $0.2g$. These acceleration magnitudes are consistent with sizeable earthquakes characteristic of vol-

canoes. The 1975 Kalapana earthquake ($M_s$ of 7.2) and the 1983 Kaoiki ($M_s$ of 6.6) earthquake are merely the most recent of events of sufficient size to cause structural damage and to influence the stability of shallow slopes [*Tilling et al.*, 1976; *Buchanan-Banks*, 1987].

The influence of lateral acceleration on stability may be gauged by incorporating the pseudostatic influence on the limit equilibrium relation of equation (27). This is achieved by resolving the components of the lateral acceleration, applied to the slide mass, perpendicular and parallel to the failure plane. Correspondingly, the numerator term of equation (27) is transformed as $\bar{M}\cos\alpha \rightarrow \bar{M}(\cos\alpha + \delta\sin\alpha)$ and the denominator as $-\bar{M}\sin\alpha \rightarrow -\bar{M}(\sin\alpha - \delta\cos\alpha)$. The pseudostatic effect is to increase the outward destabilizing force while simultaneously affecting the shear resistance on the failure plane. For shallow failure these processes act additively to reduce the factor of safety; for deep-seated failure with updip sliding, shear resistance is increased with the destabilizing seismic load.

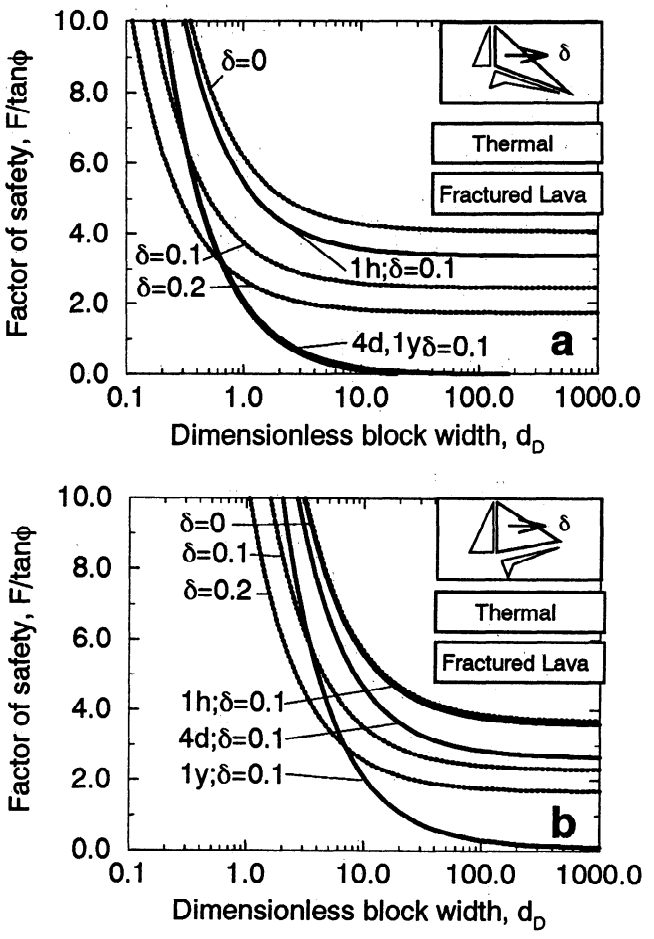


**Figure 10.** Evaluation of stability with maximum thermal effect with $A_D = 24$ and $D = 0.2 \times 10^{-3}$. (a) Variation of normalized factor of safety for shallow failure of a volcano flank subject to lateral pseudostatic earthquake acceleration, $\delta$, and with only static groundwater (dotted) and with the combined effect of static groundwater and thermally induced pore fluid pressures (solid) applied. Magmastatic pressures are applied for all analyses. Geometry with $h_m/h_s = 1$. Basal failure plane is inclined at $\alpha = -6°$. (b) Variation of normalized factor of safety for deep-seated failure of a volcano flank subject to lateral pseudostatic earthquake acceleration, $\delta$, and with only static groundwater (dotted) and with the combined effect of static groundwater and thermally induced pore fluid pressures (solid) applied. Magmastatic pressures are applied for all analyses. Geometry with $h_m/h_s = 10$. Basal failure plane is inclined at $\alpha = +6°$.

The destabilizing influence on shallow failure is examined in Figure 10a. Pseudostatic accelerations of $0.1g$ and $0.2g$ are applied to the conventional geometry with static groundwater pressures, and magmastatic pressures on the rear scarp also applied. The influence is to reduce stability with increased acceleration magnitude, especially for blocks with relatively large width where the influence of side restraint is diminished. Where the $0.1g$ acceleration is superimposed upon the already destabilizing thermal effect, the potential for failure becomes apparent, even after relatively small periods of exposure to heating (of the order of hours to days). In the configuration of shallow block geometries, the duration of acceleration in excess of some threshold value [*Newmark*, 1965] will cause displacements that may ultimately result in long runout instabilities.

The stability of deep-seated blocks is examined for quasi-static loading in Figure 10b. For these very large volume instabilities, lateral accelerations also decrease stability over the static case. Where lateral accelerations are superposed over the thermal effect, failure may result for short exposures (days to weeks) to thermal forcing. For deep block systems, the scale of the basal plane reduces the destabilizing thermal influence over that for the smaller shallow failure planes. Destabilization takes longer to develop.

For the updip failure geometry required for deep-seated failure, seismically induced instability is less pronounced than for shallow failures. In the former, the seismic acceleration increases the shear resistance on the updip failure plane, and consequently, incremental outward displacements of the block are less likely to accrue than for downdip failure.

## Conclusions

There exists a clear potential for the development of voluminous flank failures of active volcanoes as a result of dike intrusion. Our mechanistic approach shows the destabilizing influence of pore pressures induced around intruding dikes by the complementary influence of mechanical and thermal strains. Using materials and geometric parameters appropriate to oceanic shield volcanoes, analysis indicates that each of these mechanisms may trigger large-scale failures. As the mechanical and thermal loading mechanisms act on different timescales, the two may be considered in isolation. For mechanical loading, pore pressures develop close to the intrusion and, for the case of volcaniclastic materials, result in potentially destabilizing uplift force magnitudes that are

indexed relative to intrusion rate and the width of the intrusion.

Thermally induced pore pressures appear capable of developing large uplift forces beneath a potentially unstable block, with the disturbing magnitude related to the time since intrusion. Where the dike acts as a feeder over a sustained period of several days or more, the potential to trigger failure seems clear. Similar processes may apply to hydrothermal systems, even in cases for which slope failure is not accompanied by volcanism.

Once initiated, driving forces due to magma pressure will drop, and the potential to sustain failure must be examined in light of a potential reduction in shear resistance. Pore pressure enhancement may result from undrained shearing, from frictional heating, and from other mechanisms. Consequently, the development of prodigious "debris avalanche" type submarine landslides appears reasonable, provided the landslides are vigorously initiated.

Generation of suprahydrostatic pore pressures through these mechanical and thermal mechanisms also appears capable of initiating deep-seated failure involving limited slip of volcano flanks. The development of limited ruptures proximal to the zone of dike injection appears likely; these events may be seismic, and the associated seismic energy release may be enhanced by mechanical or thermal fluid pressurization mechanisms. Also, the resulting seismicity may add significantly to the destabilizing forces for more shallow seated failures. Deep seismicity also may contribute to shaking-induced fluid pressurization in the near surface zone, and this phenomenon may aid runout of shallow slides.

Only eruptive events of a sufficient critical severity appear capable of precipitating failure where, as a result of lateral restraint, the size of the failing block is constrained between minimum and maximum volumes. Minimum volume is conditioned by the influence of lateral frictional restraint, and maximum volume is influenced by the finite length of the intruded dike. The site-specific stratigraphy and structure of individual blocks are paramount, as weak layers or zones with specific material properties control the pressurization response to intrusive events. Critical block widths for the oceanic shield type volcanoes appear in the range of kilometers to tens of kilometers, and this is consistent with evidence from the Hawaiian Islands and elsewhere.

## Appendix: Dimensionless Free Body Forces

The nondimensional forces acting on the wedge geometry of Figure 3 are defined in the following. All forces have been multiplied by the quantity $d/\gamma_w h_s^3$ to yield the identities given below. These quantities represent the dimensionless block mass, $\bar{M}$, as

$$\bar{M} = \frac{1}{2}\frac{h_m}{h_s}\frac{l}{h_s}\frac{\gamma_r}{\gamma_w}\frac{d}{h_s},$$

the dimensionless force applied by seawater loading on the submerged block toe, $\bar{F}_s$, as

$$\bar{F}_s = \frac{1}{2}\frac{a}{h_s}\frac{l_s}{h_s}\frac{d}{h_s},$$

the dimensionless uplift force due to static groundwater pressures, $\bar{F}_{ps}$, as

$$\bar{F}_{p_s} = \frac{1}{2}\left(\frac{b}{h_s} + \frac{a}{h_s}\right)\frac{l_b}{h_s}\frac{d}{h_s},$$

and the dimensionless force applied by restraint on the lateral faces of the block, $\bar{F}_{pl}$, as

$$\bar{F}_{p_l} = 2\frac{1}{6}k_0\left[\frac{h_m^2}{h_s^2}\frac{l}{h_s}\frac{\gamma_r}{\gamma_w} - \frac{l_1}{h_s}\frac{b^2}{h_s^2}\right].$$

The magnitudes of forces exerted by magma and mechanically and thermally induced fluid pressures are dependent on the intrusion geometry. Planar dike geometry is used in this analysis, as represented in Figure 1.

### Magma Forces

Total dimensionless magma force, $\bar{F}_m$, acting at the rear scarp is the sum of magmastatic, $\bar{F}_{ms}$, and overpressured components, $\bar{F}_{mo}$, as

$$\bar{F}_m = \zeta(\bar{F}_{ms} + \bar{F}_{mo})$$

where $\zeta = \frac{1}{2}$ for mechanically induced pore pressure geometry and $\zeta = 1$ for the thermally induced pore pressure geometry, with

$$\bar{F}_{ms} = \frac{1}{2}\frac{\gamma_m}{\gamma_w}\left(\frac{h_m}{h_s}\right)^2\frac{d}{h_s},$$

and

$$\bar{F}_{mo} = \frac{h_m}{h_s}\frac{h_o}{h_s}\frac{\gamma_m}{\gamma_w}\frac{d}{h_s}.$$

### Mechanically Induced Fluid Pressures

The dimensionless magnitude of uplift force, $\bar{F}pm$, generated by mechanical effects, resulting from intrusion is defined as

$$\bar{F}_{pm} = \frac{w_D}{\cos\alpha}\int_{-\frac{1}{2}d_D}^{+\frac{1}{2}d_D}\int_{\frac{1}{2}U_D d_D}^{U_D\bar{R}_D} K_0[\eta]e^{\eta\frac{x_D}{\bar{R}_D}}\frac{R_D}{z_D}d\eta dx_D$$

where

$$U_D = \frac{Uh_s}{2c}; \qquad d_D = \frac{d}{h_s}.$$

### Thermally Induced Fluid Pressures

The dimensionless magnitude of uplift force, $\bar{F}_{pt}$, generated by thermal effects, resulting from magma intrusion is defined as

$$\bar{F}_{pt} = \frac{d}{h_s}\frac{ADK_b}{\gamma_w h_s}\frac{1}{\sqrt{\pi}}\sqrt{\frac{4\kappa t}{h_s^2}}\frac{1}{D\cos\alpha}.$$

The corresponding geometric relationships for the wedge geometries of Figures 3 and 4 are also defined for positive $\alpha$, for updip movement with failure, and negative $\alpha$, for downdip movement with failure. These geometric coefficients are

$$\begin{aligned}
\frac{l_b}{h_s} &= \frac{h_m}{h_s}\frac{\cos\beta}{\sin(\beta+\alpha)}, \\
\frac{l}{h_s} &= \frac{l_b}{h_s}\cos\alpha, \\
\frac{a}{h_s} &= \frac{h_m}{h_s} - \frac{l_b}{h_s}\sin\alpha - 1, \\
\frac{b}{h_s} &= \frac{h_m}{h_s} - 1 + \frac{\tan\theta}{\tan\beta}, \\
\frac{l_s}{h_s} &= \frac{a}{h_s}\frac{1}{\sin\beta}, \\
\frac{l_1}{h_s} &= \frac{l}{h_s}\frac{1}{1+\frac{a}{h_s}}, \\
\frac{l_2}{h_s} &= \frac{l_s}{h_s}\sin(\alpha+\beta).
\end{aligned}$$

## Notation

$A$ thermal strain ($\alpha\Delta T$).

$c$ hydraulic diffusivity.

$d, d_D$ width of failing block, dimensionless block width.

$D$ ratio of thermal to hydraulic diffusivity (equation (18)).

$h_m, h_s$ magma column height at dike contact, height of slope crest above sea level.

$k_0$ coefficient of earth pressure at rest, $k_0 = \sigma_h/\sigma_v$.

$k$ intrinsic permeability.

$K_b$ undrained bulk skeletal modulus of the solid.

$l, l_D, \bar{l}$ length along basal failure plane, perpendicular to the rear dike, dimensionless length ($l/h_s$), and maximum length of basal failure plane.

$n$ porosity.

$N, S$ normal and shear forces acting on the failure plane.

$p, p_s$ pore fluid pressure at a point, initial static pore fluid pressure and resulting induced pore fluid pressure ($p - p_s$).

$P_D^m, P_D^t$ dimensionless fluid pressure induced by mechanical strain (equation(2)), and induced by thermal strain (equation-(17)).

$R, R_D$ minimum radius from dike front to point where pressure is defined, dimensionless radius ($R/h_s$) (equation (5)).

$t, t_D$ time since intrusion, dimensionless time (equation(19)).

$F$ factor of safety.

$U, U_D$ dike advance rate, dimensionless advance rate (equation(3)).

$w, w_D$ dike width, dimensionless dike width (equation(7)).

$x, y, z$ coordinates fixed to migrating dike front (equation(4)).

$x_D, y_D, z_D$ dimensionless coordinates $1/h_s(x, y, z)$.

$\alpha$ inclination of basal failure surface.

$\gamma_r, \gamma_m, \gamma_w$ unit weight of rock, magma, water.

$\mu$ fluid dynamic viscosity.

$\eta$ dummy variable of integration, equal to $U_D R_D$.

$\kappa$ thermal diffusivity of saturated rock.

$\phi$ angle of internal friction along failure plane.

$\delta$ seismic acceleration relative to gravity ($+\delta g$).

**Acknowledgments.** This work was supported, in part, by the National Science Foundation under grants EAR-9106134, EAR-91173396, MSS-9218547, and EAR-9316739. This support is gratefully acknowledged. We thank W. Meyer for assistance with technical data. Thoughtful reviews by D. Swanson, A. Rubin, and A. Borgia similarly contributed to the manuscript.

## References

Ambraseys, N. N., and S. K. Sarma, The response of earth dams to strong earthquakes, *Geotechnique, 17,* 181-213, 1967.

Ando, M., The Hawaii earthquake of November 29, 1975: Low dip angle faulting due to forceful injection of magma, *J. Geophys. Res., 84,* 7611-7626, 1979.

Björnsson, A., L. Kristjánson, and H. Johnson, Some observations of the Heimacy deep drill hole during the eruption of 1973, *Jökul, 26,* 52-57, 1977.

Bodvarsson, G. S., S. M. Benson, O. Sigurdsson, V. Stefánsson, and E.T. Eliasson, The Krafla Geothermal Field, Iceland, 1, Analysis of well test data, *Water Resour. Res., 20*(11), 1515-1530, 1984.

Brandsdóttir, B., and P. Einarsson, Seismic activity associated with the September 1977 deflation of the Krafla central volcano in north-eastern Iceland, *J. Volcanol. Geotherm. Res., 6,* 197-212, 1979.

Buchanan-Banks, J. M., Structural damage and ground failure from the November 16, 1983 Kaoiki earthquake, Island of Hawaii, in Volcanism in Hawaii, edited by R. W. Decker, T. L. Wright, and P. H. Stauffer, *U.S. Geol. Surv. Prof. Pap., 1350,* 1187-1195, 1987.

Cleary, M. P., Fundamental solutions for a fluid- saturated porous solid, *Int. J. Solids Struct., 13,* 785-806, 1977.

Cleary, M. P., Moving singularities in elasto-diffusive solids with application to fracture propagation, *Int. J. Solids Struct., 14,* 81-97, 1978.

Decker, R. W., Dynamics of Hawaiian volcanoes, in Volcanism in Hawaii, edited by R. W. Decker, T. L. Wright, and P. H. Stauffer, *U.S. Geol. Surv. Prof. Pap., 1350,* 997-1018, 1987.

Delaney, P. T., Rapid intrusion of magma into wet rock: Groundwater flow due to pore pressure increases, *J. Geophys. Res., 87,* 7739-7756, 1982.

Delaney, P. T., and D. D. Pollard, Deformation of host rocks and flow of magma during flow of minette dikes and

breccia-bearing intrusions near Ship Rock, New Mexico, *U.S. Geol. Surv. Prof. Pap., 1202,* 1-61, 1981.

Dieterich, J. T., Growth and persistence of Hawaiian volcanic rift zones, *J. Geophys. Res., 93,* 4258-4270, 1988.

Duffield, W. A., L. Stieltjes, and J. Varet, Huge landslide blocks in the growth of Piton de la Fournaise, la Réunion and Kilauea volcano, Hawaii, *J. Volcanol. Geotherm. Res., 12,* 147-160, 1982.

Elsworth, D., Dislocation analysis of penetration in saturated porous media, *J. Eng. Mech. Div. Am. Soc. Civ. Eng., 117*(2), 391-408, 1991.

Elsworth, D., and A. R. Piggott, Hydrofracture characterization through the monitoring of induced pore fluid pressures, in *Proceedings of the International Conference on Flow Through Porous Media: Fundamentals and Reservoir Engineering Applications,* pp. 89-92, Institute for Problems in Mechanics, Russian Academy of Sciences, Moscow, 1992.

Elsworth, D., and B. Voight, Theory of dike intrusion in a saturated porous solid, *J. Geophys. Res., 97,* 9105-9117, 1992.

Fairbridge, R. W., Landslide patterns on oceanic volcanoes and atolls, *Geogr. J., CXV,* 84-88, 1950.

Goodman, R. E. and Y. Ohnishi, Undrained shear tests on jointed rock, *Rock Mech. Rock Eng., 5*(3), 129-149, 1973.

Gucwa, P. R. and R. O. Kehle, Bearpaw Mountains rockslide, Montana, USA, in *Rockslides and Avalanches, vol. 1: Natural Phenomena,* edited by B. Voight, pp. 393-421, Elsevier Science, New York, 1978.

Hall, J., On the vertical position and convolutions of certain strata, and their relation with granite, *Trans. R. Soc. Edinburgh, 7,* 79-108, 1815.

Hill, D. P. and J. J. Zucca, Geophysical constraints on the structure of Kilauea and Mauna Loa Volcanoes and some implications for seismomagmatic processes, in Volcanism in Hawaii, edited by R. W. Decker, T. L. Wright, and P. H. Stauffer, *U.S. Geol. Surv. Prof. Pap., 1350,* 903-917, 1987.

Holcomb, R. T. and R. C. Searle, Large landslides from oceanic volcanoes, *Mar. Geotechnol., 13,* 19-32, 1993.

Hutchinson, J. N. and R. K. Bhandari, Undrained loading as a fundamental mechanism of mudflows and other mass movements, *Geotechnique, 20,* 412-438, 1971.

Iverson, R. M., Failure and runout of giant landslides on Hawaiian volcanoes: Cases of enigmatic mechanics? *Geol. Soc. Am. Abstr. Programs, 47,* A125, 1991.

Iverson, R. M., Rigid-wedge models for metastable flanks of Hawaiian volcanoes, (abstract), *Eos Trans. AGU, 73*(43), Fall Meeting suppl., 505, 1992.

Iverson, R. M., Can magma-injection and groundwater forces cause massive landslides on Hawaiian volcanoes? *J. Volcanol. Geotherm. Res.,* in press, 1995.

Iverson, R. M. and R. G. LaHusen, Dynamic pore-pressure fluctuations in rapidly shearing granualr materials, *Science,* 246, 796-799, 1989.

Keefer, D. K., Landslides caused by earthquakes, *Geol. Soc. Am. Bull., 95,* 406-421, 1984.

Koyanagi, R. Y., D. A. Swanson, and E. T. Endo, Distribution of earthquakes related to the mobility of the south flank of Kilauea Volcano, Hawaii, in Geological Survey Research 1972, *U.S. Geol. Surv. Prof. Pap., 800-D,* D89-D97, 1972.

Labazuy, P., and J.-F. Lénat, Recurrent landslides on the east flank of Piton de la Fournaise Volcano, Réunion, *Eos Trans. AGU, 71*(43), Fall Meeting suppl., 1577, 1990.

Lambe, T. W. and R. V. Whitman, *Soil Mechanics, SI Version,* 553 pp., John Wiley, New York, 1979.

Lénat, J.-P., P. Vincent, and P. Bachelery, The offshore continuation of an active basaltic volcano: Piton de la Fournaise (Réunion Island, Indian Ocean), *J. Volcanol. Geotherm. Res., 36,* 1-36, 1989.

Lipman, P. W., J. P. Lockwood, R. T. Okamura, D. A. Swanson, and K. M. Yamashita, Ground deformation associated with the 1975 magnitude 7.2 earthquake and resulting changes in activity of the Kilauea volcano, Hawaii, *U.S. Geol. Surv. Prof. Pap., 1276,* 45 pp., 1985.

Mink, J. F., and L. S. Lau, Hawaiian groundwater geology and hydrogeology, and early mathematical models, *U.S. Geol. Surv. Tech. Memo. Rep., 62,* 14 pp., 1980.

Moore, J. G., Giant submarine landslides on the Hawaiian Ridge, *U.S. Geol. Surv. Prof. Pap., 501-D,* D95-D98, 1964.

Moore, J. G. and R. S. Fiske, Volcanic substructure inferred from dredge samples and ocean-bottom photographs, Hawaii, *Geol. Soc. Am. Bull., 80,* 1191-1202, 1969.

Moore, J. G., and H. L. Krivoy, The 1962 flank eruption of Kilauea volcano and structure of the east rift zone, *J. Geophys. Res., 69,* 2033-2045, 1964.

Moore, J. G., D. A. Clague, R. T. Holcomb, P. W. Lipman, W. R. Normark, and M. E. Torresan, Prodigious submarine landslides on the Hawaiian Ridge, *J. Geophys. Res., 94,* 17465-17484, 1989.

Newmark, N. M., Effects of earthquakes on dams and embankments, *Geotechnique, 15,* 139-159, 1965.

Ouyang, Z., An investigation of dislocations propagating in poroelastic media, Ph.D. thesis, 128 pp., Pa. State Univ., University Park, 1994.

Pariseau, W. G., and B. Voight, Rockslides and avalanches: Basic principles and perspectives in the realm of civil and mining operations, in *Rockslides and Avalanches,* vol. 2, *Engineering Sites,* edited by B. Voight, pp. 1-92, Elsevier Science, New York, 1979.

Prostka, H. J., Heart Mountain fault and Absaroka volcanism, in *Rockslides and Avalanches,* vol. 1, *Natural Phenomena,* edited by B. Voight, pp. 423-437, Elsevier Science, New York, 1978.

Rice, J. R., and M. P. Cleary, Some basic stress diffusion solutions for fluid-saturated elastic porous media with compressible constituents, *Rev. Geophys., 14*(2), 227-241, 1976.

Rubin, A. M. and D. D. Pollard, Origins of blade-like dikes in volcanic rift zones, Volcanism in Hawaii, edited by R. W. Decker, T. L. Wright, and P. H. Stauffer, *U.S. Geol. Surv. Prof. Pap., 1350,* 1449-1470, 1987.

Rudnicki, J. W., On "Fundamental solutions for a fluid-saturated porous solid" by M. P. Cleary, *Int. J. Solids Struct., 17,* 855-857, 1981.

Sassa, K., Geotechnical model for the motion of landslides, in *Proceedings of the Fifth International Symposium on Landslides,* pp. 37-55, A. A. Balkema, Rotterdam, 1988.

Seed, H. B., Considerations in the earthquake-resistant design of earth and rockfill dams, *Geotechnique, 29*(3), 213-263, 1979.

Seed, H. B., Earthquake-resistant design of earth dams, in *Proceedings of the Third International Conference on Recent Advances in Geotechnical Earthquake Endineering and Soil Dynamics,* pp. 1157-1175, University of Missouri, Rolla, 1981.

Seed, H. B., K. L. Lee, and I. M. Idriss, Analysis of Sheffield dam failure, *J. Soil Mech. Found. Div. Am. Soc. Civ. Eng., 95,* 1453-1490, 1969.

Sigurdsson, O., Analysis of pressure pulses resulting from volcanic activity in the vicinity of a well, M.S. thesis, 72 pp., Univ. of Okla., Norman, 1982.

Skempton, A. W., The pore-pressure coefficients A and B, *Geotechnique, 4,* 143-147, 1954.

Stearns, H. T., and G. A. Macdonald, Geology and groundwater resources of the island of Hawaii, *Hawaii Div. Hydrogr. Bull., 9,* 363 pp., 1946.

Stefánsson, V., The Krafla geothermal field, northern Iceland, in *Geothermal Systems; Principles and Case Histories,* edited by L. Rybach and L. J. P. Muffler, pp. 273-294, John Wiley, New York, 1981.

Swanson, D. A., W. A. Duffield, and R. S. Fiske, Displacement of the South flank of Kilauea Volcano: The result of forceful intrusion of magma into the rift zone, *U.S. Geol. Surv. Prof. Pap., 963,* 39 pp., 1976.

Terzaghi, K., Mechanisms of landslides, in *Application of Geology to Engineering Practice, Berkey Volume,* edited by S. Paige, pp. 83-123, Geological Society of America, Boulder, Colo. 1950.

Thomas, D., A geochemical model of the Kilauea east rift zone, in Volcanism in Hawaii, edited by R. W. Decker, T. L. Wright, and P. H. Stauffer, *U.S. Geol. Surv. Prof. Pap., 1350,* 1507-1525, 1987.

Tilling, R. I., R. Y. Koyanagi, P. W. Lipman, J. P. Lockheed, J. G. Moore, and D. A. Swanson, Earthquakes and related catastrophic events, Island of Hawaii, November 29, 1975: A preliminary report, *U.S. Geol. Surv. Circ., 740,* 33 pp., 1976.

Tryggvason, E., Subsidence events in the Krafla area, north Iceland, 1975-1979, *J. Geophys., 47,* 141-153, 1980.

Voight, B., Fluid-wedge hypothesis and the Heart Mountain and Reef Creek décollements, northwestern Wyoming, USA, *Geol. Soc. Am. Abstr. Programs, 4,* 698, 1972.

Voight, B., and D. Elsworth, Resolution of mechanics problems for prodigious Hawaiian landslides: Magmatic intrusions simultaneously increase driving force and reduce driving resistance by fluid pressure enhancement (abstract), *Eos Trans. AGU, 73*(43), Fall Meeting suppl., 506, 1992.

Voight, B., and C. Faust, Frictional heat and strength loss in some rapid landslides, *Geotechnique, 32,* 43-54, 1982.

Voight, B., and J. Sousa, Lessons from Ontake-san: A comparative analysis of debris avalanche dynamics, *Eng. Geol., 38,* 261-297, 1994.

Voight, B., R. J. Janda, H. Glicken and P. M. Douglass, Nature and mechanics of the Mount St. Helens rockslide-avalanche of 18 May 1980, *Geotechnique, 33,* 243-273, 1983.

Watanabe, H., Changes in water level and their implications to the 1977-1978 activity of Usu volcano, in *Arc Volcanism: Physics and Tectonics,* edited by D. Shimozuru and J. Yokoyama, pp. 81-93, Terra Scientific, Tokyo, 1983.

Ylinen, A. M., and D. Elsworth, Heat and mass transfer around an advancing penetrometer, *Int. J. Heat Mass Trans., 34,* 1407-1416, 1991.

Zucca, J. J., and D. P. Hill, Crustal structure of the southeast flank of Kilauea Volcano, Hawaii, from seismic refraction measurements, *Bull. Seismol. Soc. Am., 70,* 1149-1159, 1980.

Zucca, J. J., D. P. Hill, and R. L. Kovach, Crustal structure of Mauna Loa Volcano, Hawaii, from seismic refraction measurements and gravity data, *Geol. Soc. Am. Bull., 72,* 1535-1550, 1982.

---

D. Elsworth, Department of Mineral Engineering, Pennsylvania State University, University Park, PA 16802-5000. (e-mail: elsworth@pnge.psu.edu)

B. Voight, Department of Geosciences, Pennsylvania State University, University Park, PA 16802-2712. (e-mail: voight@ems.psu.edu)

(Received March 21, 1994; revised October 24, 1994; accepted November 2, 1994.)